uOttawa

Mapping Wild Leek with UAV and Satellite Remote Sensing

Edmar Miglhorance

Thesis submitted to the Faculty of Graduate
and Postdoctoral Studies in partial fulfillment of the requirements
for the M.Sc. Degree in Physical Geography

Department of Geography, Environment and Geomatics
Faculty of Arts
University of Ottawa

Supervisor:
Dr. Anders Knudby

Thesis Committee:
Dr. Luke Copland
Dr. Michael Sawada

Abstract

Wild leek (*Allium tricoccum*) is a spring ephemeral of northeastern North America. In the Canadian province of Quebec, it is listed as threatened due to human harvesting, and in Gatineau Park its presence is used as an indicator of human impact. Wild leek grows in patches on the forest floor, and before the tree canopy develops its green leaves are clearly visible through the bare branches of deciduous forests, allowing it to be observed with optical remote sensing. This study developed and tested a new method for monitoring wild leek across large geographic areas by integrating field observations, UAV video, and satellite imagery. Three-cm resolution orthomosaics were generated for five <0.1 km^2 sites from the UAV video using Structure-from-Motion, segmented, and classified into wild leek (WL) or other (OT) surface types using a simple greenness threshold. The resulting maps, validated using the field observations, had a high overall accuracy (F1-scores between 0.64 to 0.94). These maps were then used to calibrate a linear model predicting the per-pixel percentage cover of wild leek (%WL) from NDVI in the satellite imagery. The linear model calibrated for a Sentinel-2 image from 2018, covering all of Gatineau Park (~361 km^2), allowed %WL to be predicted with an RMSE of 10.32. A similar model calibrated for a WorldView-2 image from 2018 was noisy (RMSE = 37.64), though much improved by resampling this image to match the spatial resolution of Sentinel-2, due to MAUP scale effect (RMSE = 13.06). Testing the potential for satellite-based monitoring of wild leek, the %WL prediction errors were similar when a new linear model was developed using the Sentinel-2 image from 2017 (RMSE = 12.84) and when the model calibrated with the 2018 Sentinel-2 image was applied to the 2017 satellite data (RMSE = 16.97). The linear models developed for the Sentinel-2 and WorldView-2 images from 2018 were used to map wild leek cover for Gatineau Park. Both images allowed production of similar wild leek maps that, based on field experience and visual inspection of the imagery, provide good descriptions of the actual distribution of wild leek at Gatineau Park.

Acknowledgments

Foremost, I would first like to express my most sincere gratitude to Dr. Anders Knudby for his patience, motivation, generosity and guidance that helped me all the time during my Master's program. I could not have imagined having a better advisor and mentor. Thank you very much for your support and understanding. I will be forever grateful to you.

I would also like to thank my thesis committee: Dr. Luke Copland and Dr. Michael Sawada, for their comments, suggestions and advice in completing this project.

Finally, I would like to thank my Brazilian and Canadian family and friends for believing in me every step of the way; I could not have achieved any of this without their support. Last but certainly not the least, I would like to thank Heenie for his continuous encouragement, for listening to me every day, and for never letting me doubt myself. This accomplishment would not have been possible without them. Thank you!

Table of Contents

List of Tables

List of Figures

1 Introduction

Wild leek (*Allium tricoccum*) is a spring ephemeral of deciduous forests of northeastern North America [1–3] that is harvested for its edible bulbs [3,4]. As a result of overharvesting over the last few decades, many populations of wild leek have declined in the Canadian province of Quebec, and some in Southern Quebec have disappeared [2,5]. In Quebec, wild leek is considered a vulnerable plant species according to the Regulation Respecting Threatened or Vulnerable Wild Species and Their Habitats [5,6].

Wild leek takes advantage of a short period of time immediately after snow melt to develop its leaves when solar irradiance is maximal on the forest floor (typically from late April to early May in Southern Quebec). After the forest canopy has closed (typically late May or early June), the leaves senesce and decompose [1,4]. Wild leek can thus only be seen through the tree canopy during a 5-6-week period in late spring/early summer [3,4].

Patches of wild leek grow under the bare branches of deciduous forests, normally in areas well exposed to light. As opposed to other spring ephemerals that tend to grow in a more scattered pattern, wild leek can form dense patches covering large areas [7].

Monitoring wild leek population dynamics is necessary for management at a large scale [3]. Due to field-based observations being time-consuming and labor-intensive, and therefore expensive, monitoring wild leek over broad areas is a challenge. Remote sensing is a cost-effective alternative to field observations when covering large areas, and is thus a potential solution for wild leek monitoring, but methods for monitoring of patchy understory vegetation are not well-developed. Testing the ability of different platforms (Unmanned Aerial Vehicles (UAVs), aircraft, satellites) and sensors (multispectral, hyperspectral) is necessary to develop a method appropriate for mapping and monitoring wild leek.

1.1 Thesis Objective

This thesis aims to develop and test a new method for monitoring wild leek across large geographic areas. Combining different approaches used for monitoring understory vegetation [7–9], the method integrates field data, UAV video and satellite images, and is used to produce maps of wild leek for Gatineau Park, Quebec. The method works by:

1. Creating high-resolution maps of wild leek for several small (<0.1 km^2) sites in the study area, by applying a greenness threshold to orthomosaics created from UAV-based video processed with Structure from Motion. These maps are calibrated and validated with field observations; the accuracy of this method has previously been demonstrated [7].

2. These high-resolution wild leek maps are then used to quantify the percentage of wild leek (%WL) within each pixel of a satellite image, and a linear model predicting %WL from values of NDVI found in each satellite image pixel is applied to the entire image. Two types of satellite images are used in this process, a Sentinel-2 image and a WorldView-2 image.

3. The linear model acquired for Sentinel-2 was applied to a Sentinel-2 image from a different year to test the between-year use of the model.

1.2 Thesis Format

This thesis is presented in article format, with a manuscript intended for publication. The paper "*Mapping Wild Leek with UAV and Satellite Remote Sensing*", presented in chapter 2 will be submitted to "*Remote Sensing*" for publication. Chapter 3 provides a general conclusion of outcomes presented in chapter 2. References are listed in chapter 4.

2 Mapping wild leek with UAV and Satellite Remote Sensing

2.1 Introduction

2.1.1 Wild Leek

Understory vegetation plays an essential role in forest ecosystems. Besides its contributions to forest structure and function, it provides vital resources for wildlife, such as food and protection [10–13], hence understanding the population distributions of understory species is important for forest management and environmental conservation [10]. Understory plants are also crucial for the cycling of nutrients, and are therefore often considered good indicators of forest health [12,14–16].

Under the bare branches of deciduous forests of northeastern North America, mostly composed of maple trees, the spring ephemeral species known as wild leek *(Allium tricoccum,* also known as ramps*)* can be found typically growing in dense patches, unlike other spring ephemerals species (Figure 1; [3–5,7,17,18]. Wild leek grows on moist slopes, streamside bluffs and depressions, in cool areas with soil rich in minerals and organic matter [19–23].

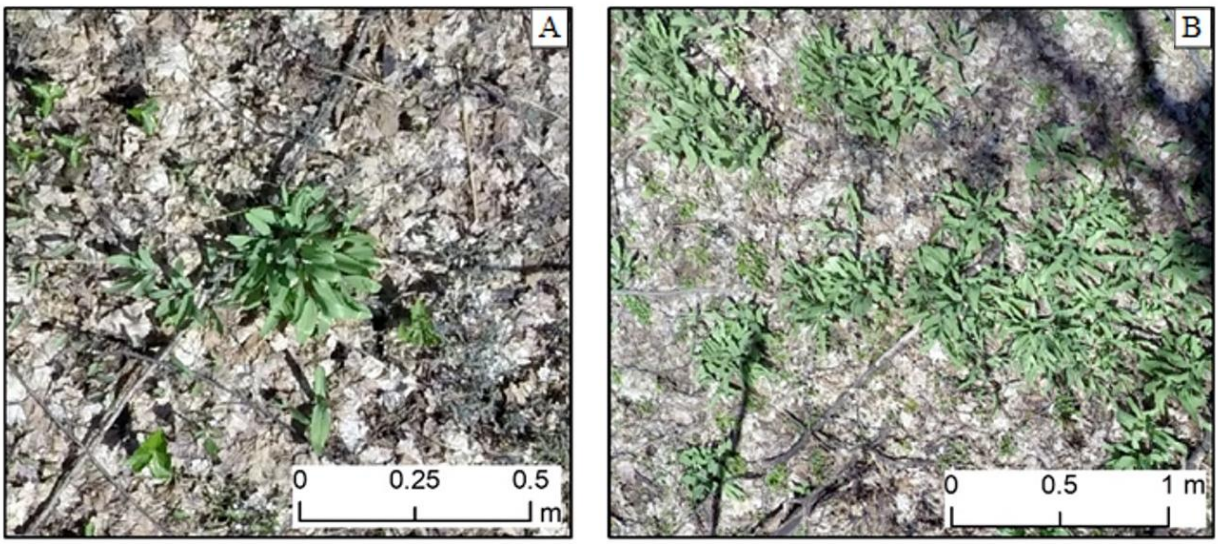

Figure 1. Small (A) and big (B) patches of wild leek in Gatineau Park - Quebec. Photos taken in 2017 from a UAV flying at low altitude.

New wild leek leaves emerge as soon as the forest floor starts to receive direct sunlight after the snow melt and the leaves commence to die and decompose once the tree canopy begins to develop and block off sunlight from reaching the forest floor [1,4,5,7,13,18–20]. The difference in phenology between understory and overstory species makes wild leek visible through the leafless tree canopy for a

period of ~5 weeks in late spring/early summer [3,7,19], during which wild leek can be detected with optical remote sensing [9,24]. In southern Quebec, Canada, this period typically falls around mid-April to mid-May [1,4].

In eastern Canada, a noticeable decline in the natural population of wild leek has been caused by overharvesting [2,3,22]. Wild leek is harvested for a variety of purposes, from personal to commercial use, as food or medication [20]. Despite being known for the flavor of its bulbs, wild leek is harvested in its entirety since both its bulb and leaves are edible [18,22]. Vegetative propagation, due to division of large ramets that produces new individuals every couple of years, is the most important method of population growth and maintenance [2,3,13]; seedlings contributes to less than 5% of population growth rate [3]. Large indivuduals of wild leek, which are responsible for most of both vegetative propagation and seed production, are also most frequently targeted for harvesting [3].

Given the growth limitations, especially the high dependence on vegetative propagation, wild leek is sensitive to harvesting and population recovery occurs slowly [2,4,18,20,22]. As a result, limits on harvesting have been imposed in Quebec [4,20]. Commercial harvesting has been banned since 1995 and harvesting for personal use is controlled under the *Act Respecting Threatened or Vulnerable Species*, which allows annual harvesting of up to 200 grams per person [1,6,20]. No harvesting is permitted in Gatineau Park, which contains one of Quebec's largest wild leek populations [3,25]. However, enforcement is difficult and harvest limits are often exceeded, and illegal harvesting still happens even within protected areas [20]. Monitoring wild leek population dynamics is therefore necessary for management at a large scale [3].

2.1.2 Mapping Understory Vegetation

Field-based mapping and monitoring of patchy understory vegetation such as wild leek is time consuming and labour-intensive, and thus costly, making it impractical for large areas [15,26–28]. The use of near-surface remote sensing with Unmanned Aerial Vehicles (UAVs) for environmental monitoring has grown substantially in recent years due to its ability to acquire high-resolution spatial data; it is often less expensive than field data collection and it can be deployed quickly and repeatedly [29–32]. Nevertheless, there are two major constraints on using UAVs for understory vegetation monitoring. First, while any kind of sensor can in principle be flown on a UAV, most UAVs, including the one used in this study, carry optical sensors with low spectral resolution that only acquire images in the red, green and blue (RGB) parts of the visible spectrum while not recording the near-infrared or shortwave-infrared wavelengths that are useful for detection and assessment of vegetation [33–35].

Second, because of the small area covered by each photo acquired from a low-flying UAV, a large number of photographs is needed to cover relatively small areas, and combining these photos in an orthomosaic, while possible to largely automate, requires substantial computing resources [29,32].

Orthomosaic generation with Structure from Motion (SfM) requires multiple overlapping photographs that together capture full the three-dimensional structure of the area [36–38]. SfM software works by identifying features recognizable in multiple images, and uses these features to orient all images relative to each other, thereby allowing triangulation of the features which are extracted as a point cloud [38]. As opposed to traditional photogrammetric approaches, SfM automatically determines both camera pose (location and orientation) and feature locations in an arbitrary coordinate system [39,40]. The feature point cloud must therefore be georeferenced by using photos or ground control points with known coordinates.

Due to the lack of a near-infrared (NIR) band in the UAV imagery and resulting orthomosaics, vegetation information must be derived from the RGB bands. Several RGB-based vegetation indices exist for this purpose, of which the Green Chromatic Coordinate (GCC) is most widely used to monitor phenological development of plants and trees [41–44] because its values are highly correlated with Normalized Difference Vegetation Index (NDVI) [42]. The GCC is calculated as the green reflectance divided by the sum of red, green and blue reflectances, and has previously been used for mapping wild leek with UAV-based imagery [7]. Vegetation indices help in the separation between the classes of interest from the other classes during classification.

Object-based image analysis (OBIA), which has previously been demonstrated as effective for analysis of UAV images [35,45–47], is more appropriate for high-resolution imagery classification than pixel-based methods [48–52]. OBIA segments the image into homogeneous objects based on their spatial and spectral characteristics [31,48,53–55], and the objects, rather than the pixels they are composed of, can then be classified [56,57].

Despite being capable of mapping wild leek within small areas (~0.06 km^2) [7], UAV-based imagery does not provide the coverage needed to map and monitor wild leek over large areas, such as Gatineau Park in southern Quebec (~361 km^2). Satellite-based observations with high/moderate spatial detail are widely used to monitor vegetation [8–11,28,47,58–60] and remain the best alternative when monitoring large areas [15,27,61,62]. However, the relatively poorer spatial resolution of satellite imagery is an important challenge since wild leek typically grows in patches smaller than 10 m^2, which is smaller than the pixel size of many satellite images. As such, despite being widely used to monitor understory vegetation, Landsat imagery is unsuitable specifically for wild leek mapping because detection of even very large wild leek patches, e.g. 10-20 m across would only cover a small fraction of

a single pixel [8,9,11,28,58,59,62–64]. Satellite data with higher spatial resolution, such as Sentinel-2, SPOT, IKONOS, QuickBird, RapidEye, WorldView and GeoEye, are likely more suitable for wild leek mapping.

Remote detection of understory vegetation is limited due to the interference of the overstory canopy [10,60]. In order to overcome this challenge, knowledge of the phenological differences between vegetation types has been used to specifically detect understory plants [7–11,28,58]. If the understory vegetation has a different leaf phenology from the overstory species, satellite images acquired during the deciduous leaf-off and understory leaf-on periods can be used to identify the presence of the understory vegetation [8,9,11,58,60]. However, coniferous tree species, which are also green during this period, can be confused with the understory vegetation. Distinguishing the understory vegetation from coniferous trees, and eliminating the latter from the analysis, is therefore crucial [9]. To do this, many studies have used two different images [8,9,58]; in addition to (a) the deciduous leaf-off and understory leaf-on image, another (b) deciduous leaf-off and understory leaf-off image is acquired. Coniferous trees, as the only green vegetation on (b), can then easily be outlined and removed from the understory leaf-on image (a).

Combining different approaches used for monitoring understory vegetation [7–9], this study aims to develop and test a new method for monitoring wild leek across large geographic areas by integrating field data, UAV video, and satellite images, and is used to produce maps of wild leek for Gatineau Park, Quebec. The method works by:

1. Creating high-resolution maps of wild leek for several small (<0.1 km^2) sites in the study area, applying a greenness threshold to orthomosaics created from UAV-based video processed with Structure from Motion. These maps are calibrated and validated with field observations; the accuracy of this method has previously been demonstrated [7].

2. These high-resolution wild leek maps are then used to quantify the percentage of wild leek (%WL) within each pixel of a satellite image, and a linear model predicting %WL from values of NDVI found in each satellite image pixel is applied to the entire image. Two types of satellite images are used in this process, a Sentinel-2 image and a WorldView-2 image.

3. The linear model acquired for Sentinel-2 was applied to a Sentinel-2 image from a different year to test the between-year use of the model.

2.2 Study Area and Data Acquisition

2.2.1 Study Area

Gatineau Park is a natural protected area located 20 km northwest of Ottawa, Canada, covering ~361 km^2 of land between the Ottawa and Gatineau rivers (Figure 2). The park is heavily used by residents and tourists all year long, with over 2.7 million visits per year, and also provides habitat for more than 5,000 species of plants and animals, including vulnerable and threatened species such as wild leek. To monitor the health of the park, given its heavy human use, Gatineau Park has been tracking a set of environmental indicators since ~2006 [65,66]. Wild leek is used, with other plant species at risk, as an indicator of the impact of recreational activities on species at risk for Gatineau Park [65] and more broadly for Parcs Québec [12].

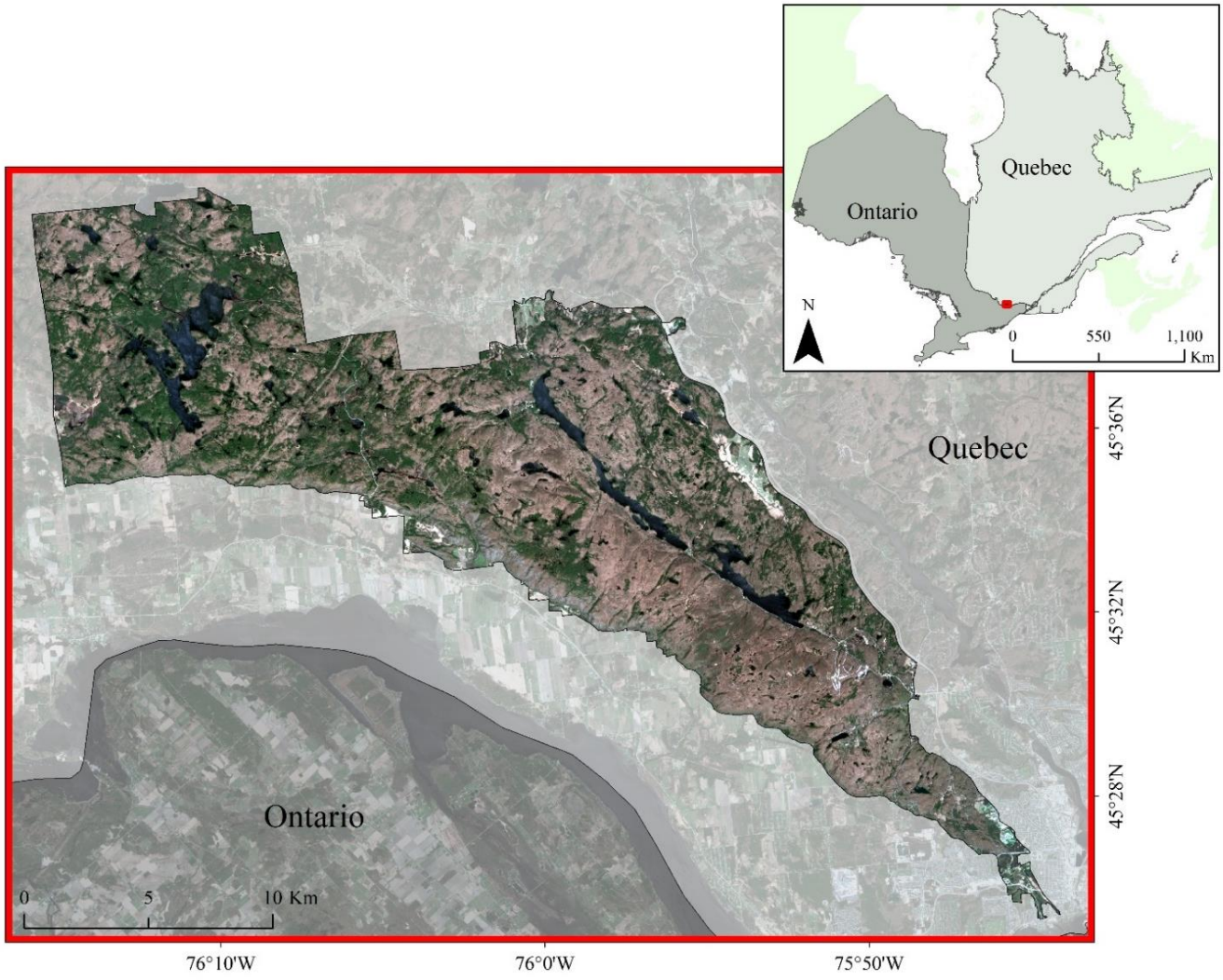

Figure 2. Location of the study area, Gatineau Park. Sentinel-2 imagery from May 9, 2018. Coordinates refer to WGS 1984.

In Gatineau Park wild leek is found predominantly in the southern portion of the park, where the forest is dominated by hardwood deciduous trees [1,7]. Wild leek in the park has benefited from legal protection from harvesting since 1980, and since 1995 the sale of wild leek has been prohibited throughout Quebec, though not in nearby Ontario [3,20,25].

2.2.2 Wild Leek Detection

Different types of vegetation have different spectral reflectance signatures, which can be used to detect and map their presence/absence, percent cover, and other attributes [61,67]. In Gatineau Park other spring ephemerals emerge simultaneously with wild leek and in similar environments, such as ferns (*Pteridophyta* sp.), white trillium (*Trillium grandiflorum*), red trillium (*Trillium erectum*), blue cohosh (*Caulophyllum thalictroides*), trout lily (*Erythronium americanum*), and squirrel corn or dutchman's breeches (*Dicentra* sp.). In comparison to these other species, wild leek has a vibrant green colour and typically develops in very dense patches over small or large areas [7]. Among all the other spring ephemeral species, white trillium is the most similar to wild leek as it also grows in patches, though at lower density and with paler green colour [7,68,69].

The acquisition of an image during the temporal window of overstory leaf-off and understory leaf-on periods has often been used to map the distribution of understory vegetation in general [8,11,58,60], and wild leek specifically [7]. Leduc & Knudby [7] acquired UAV-based imagery when wild leek could be observed directly through the leafless deciduous canopy and presented a workflow for using such imagery to map wild leek for small (~0.06 km^2) areas. Despite mapping wild leek accurately, UAV-based imagery does not provide the areal coverage needed to map and monitor wild leek for an area the size of Gatineau Park; satellite imagery is required to achieve the necessary areal coverage at reasonable cost. We therefore used the UAV-based workflow [7] to produce accurate wild leek maps for small areas, and then used those maps as input to a second workflow based on satellite imagery.

2.2.3 UAV and Ground Data Acquisition

Both UAV and ground data were acquired on 7 May 2018. Pre-programmed UAV flights were performed at 60 meters above ground, with one flight conducted for each site (Figure 3). Using a DJI Phantom 3 Standard, nadir videos were captured at 29 frames per second in 2.7k mode.

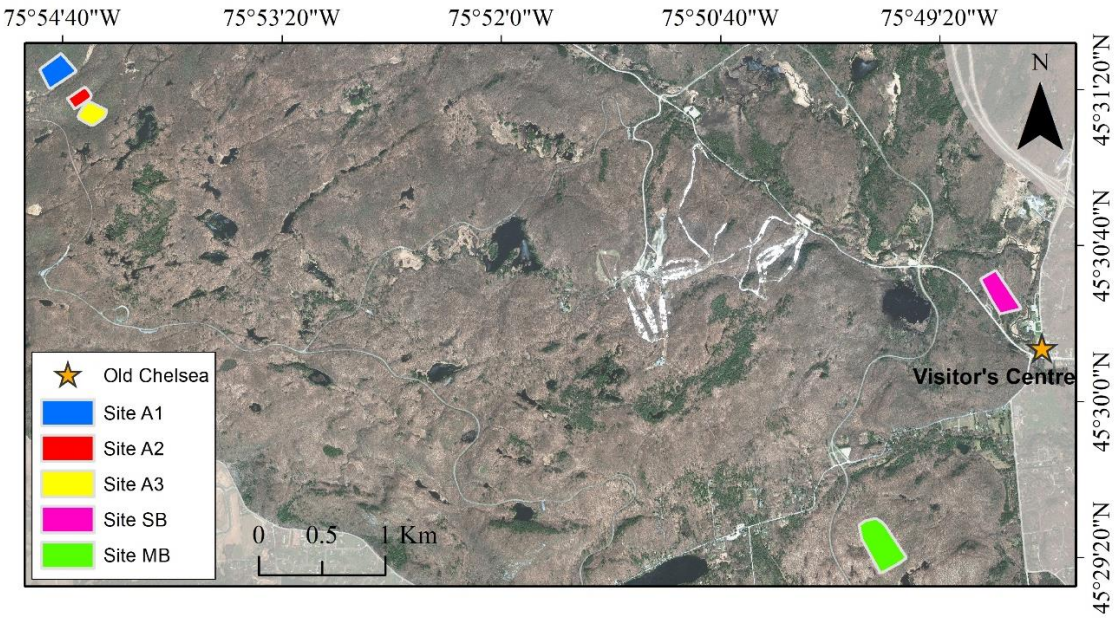

Figure 3. UAV videos were acquired for sites for sites A1, A2, A3, MB and SB.

Within each of the roughly rectangular sites, bright colorful markers were placed in each of the four corners; four markers were placed in each corner, outlining a ~10 m^2 area (Figure 4). The centres of the bright markers were used as ground control points (GCPs) for the UAV video, and their coordinates were recorded with a Trimble R1 DGPS unit, which had a typical horizontal position accuracy of 70-100 cm on the forest floor. Using a GoPro attached to the top of a ~3 m selfie-stick, near-nadir photos, in which all four corner markers were typically visible, were acquired while walking around the markers.

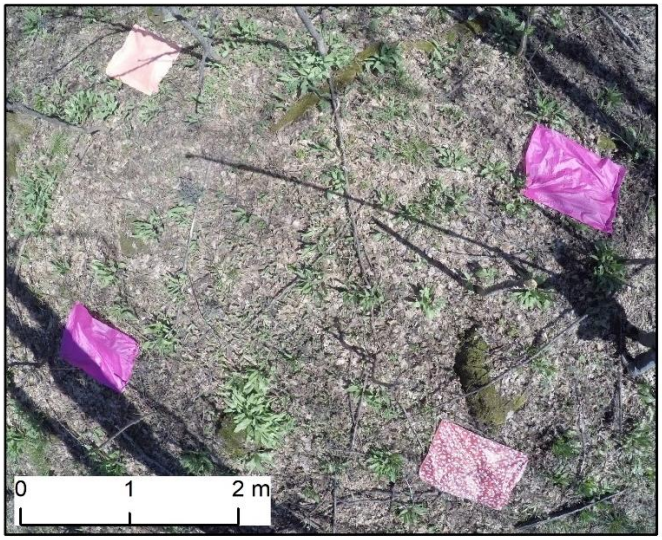

Figure 4. Photo taken with a GoPro, showing the bright markers placed in one of the corners of A1, 2018. Wild leek appears in patches with its characteristically bright green colour.

2.2.4 Satellite Data Acquisition

Both WorldView-2 and Sentinel-2 satellite images were assessed for their ability to map wild leek. WorldView-2 is representative of the current state-of-the-art in high-resolution optical satellite imagery, while Sentinel-2 is the sensor that currently produces the highest-resolution freely available satellite imagery.

Considerations for selection of specific images from each sensor included initially the time of year, as the wild leek is only visible through the leafless overstory during a period of ~5 weeks in late spring/early summer [3,4,7,19], and secondly the absence of cloud and snow in the images, which would affect the calculation of vegetation indices [42].

A total of four images were acquired, three for Sentinel-2 and one for WorldView-2. "Spring" images were acquired at a time when the green leaves of the wild leek had emerged and, in the overstory, deciduous trees were leafless and coniferous trees were green, and a "winter" image was acquired from a period when deciduous plants were devoid of leaves and coniferous trees were the only green plants in the image. While the "winter" image was acquired in March, it had necessary characteristic of coniferous trees being the only green vegetation at the time of image acquisition. To test inter-annual stability of the relationship between wild leek observations in the field and satellite imagery, two Sentinel-2 spring images were acquired, one from 2018 (the year of field data acquisition), and another one from 2017. A summary of the selected imagery is shown in Table 1.

Table 1. A summary of the imagery used in this study. The WorldView-2 imagery was obtained courtesy of DigitalGlobe Foundation. VNIR bands include the visible (RGB) bands as well as the Near-Infrared band (s).

Satellite	Acquisition Data	Acquisition Time	Spring / Winter	Spatial Resolution
WolrdView-2	May 6, 2018	11:16:44	Spring image	2 meters
Sentinel-2A	March 30, 2017	10:59:01	Winter image	10 meters (VNIR bands)
Sentinel-2A	April 29, 2017	11:10:31	Spring image	10 meters (VNIR bands)
Sentinel-2B	May 9, 2018	10:58:59	Spring image	10 meters (VNIR bands)

2.3 Data Processing

The methodology used to produce wild leek maps from WorldView-2 and Sentinel-2 satellite imagery involved the processing of field observations, UAV imagery, as well as the satellite images themselves. The complete workflow is outlined in Figure 5 and Figure 6; Figure 5 describes the use of field observations and UAV imagery to produce small-extent high-resolution wild leek maps as outlined by Leduc & Knudby [7], while Figure 6 describes how those high-resolution wild-leek maps

are combined with satellite imagery to assess its ability to map wild leek at larger spatial extents. The numbers associated with the workflow steps described in the following paragraphs all refer to Figure 5 and Figure 6.

2.3.1 Step 1: Ground Data Processing

(1.1) Ground images were acquired using a GoPro. (1.2) These images were processed using SfM framework in Agisoft PhotoScan Professional to generate three-dimensional point clouds. The point clouds were then georeferenced with the 16 GCPs recorded at each of four brightly coloured markers located in each of the four corners of the site (Figure 4). (1.3) Points located above the ground, i.e. those representing branches and tree trunks, were then manually removed from the points clouds using the selection function in Agisoft PhotoScan Professional, which allows thousands of points to be selected and removed at a time. Automatic methods to perform this step are also available, but were not tested in this study. From the remaining ground-level points 0.3-cm resolution RGB-orthomosaics were then created. The warping caused by the wide angle of GoPro's lens did not seriously affect the orthomosaic creation because the lens model is estimated and incorporated in the point location reconstruction in SfM. Moreover, the edges of the orthomosaics, areas that could have been the most affected by warping, were clipped out after orthomosaic creation since they fell outside the area between the bright coloured markers. (1.4) For each of the ground-based orthomosaics, 100 calibration points were randomly distributed and identified as either Wild Leek (WL) or Other (OT) through visual interpretation in ArcGIS. This process was completed for the four corners of each site, producing a total of 400 calibration points classified as WL or OT for each site.

2.3.2 Step 2: UAV Data Processing

(2.1) All image frames were extracted from each UAV video, and (2.2) processed through the SfM framework in Agisoft PhotoScan Professional to generate three-dimensional point clouds. Point cloud georeferencing, originally based on the internal UAV GPS information, was improved using the GCPs recorded at the bright markers for each site, which were easily identified in all point clouds. (2.3) Points located above ground were manually removed from the points cloud, and 3-cm resolution RGB-orthomosaics were generated with the remaining ground-level points. (2.4) The orthomosaics were then segmented using eCognition Developer 64 (®Trimble GeoSpatial, Munich, Germany), and (2.5) the mean GCC was calculated per segment. As the orthomosaics are not radiometrically calibrated, the GCC was calculated on the basis of raw Digital Numbers rather than reflectance values.

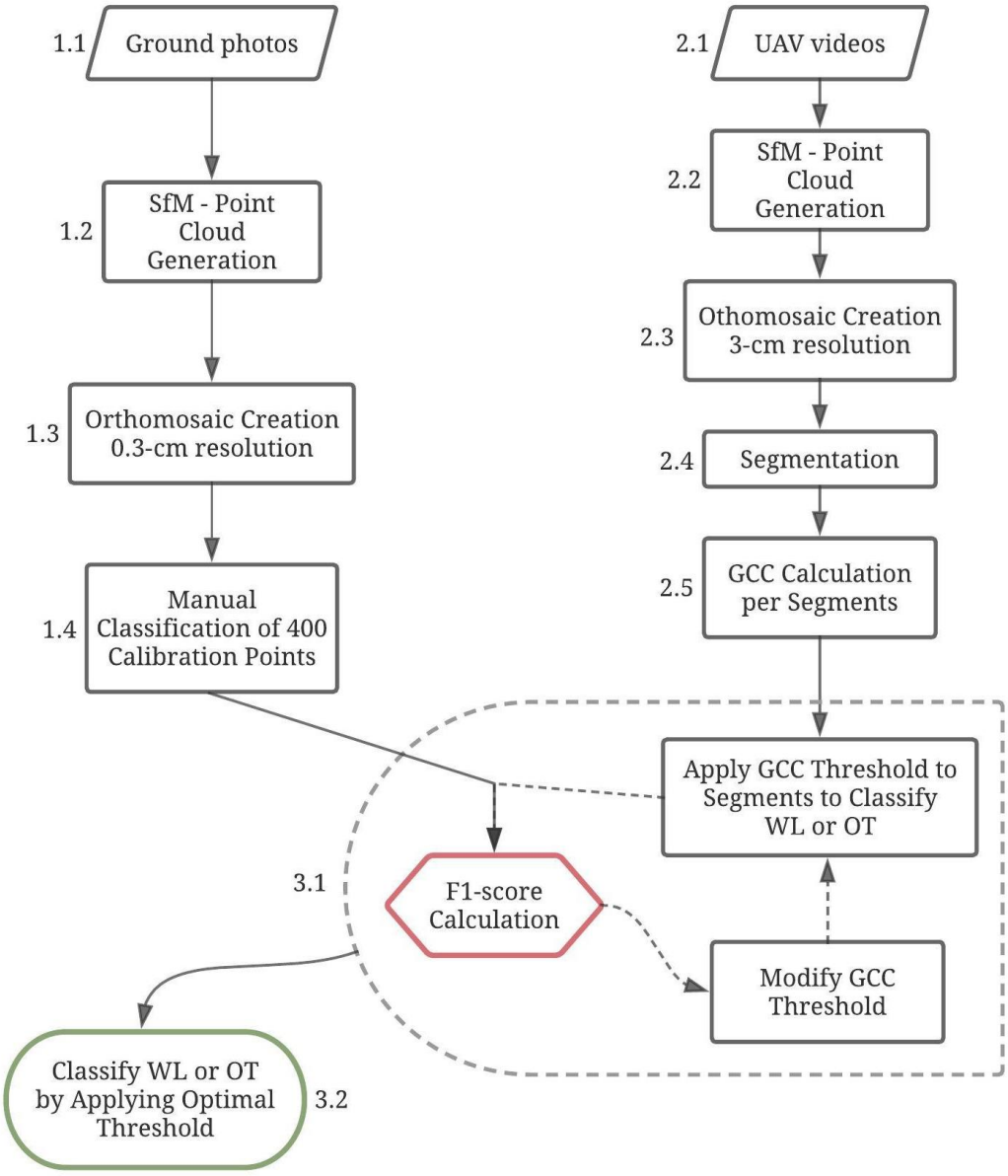

Figure 5. Workflow for processing UAV and ground data, optimizing GCC threshold used to distinguish wild leek from other surfaces, and assessing the accuracy of UAV-based wild leek classification.

2.3.3 Step 3: GCC Threshold Calibration

(3.1) For each site, in order to classify each segment as either WL or OT, a threshold was applied to the per-segment GCC values in the UAV-based orthomosaic; segments with GCC values greater than the threshold were then classified as WL, and vice-versa. The accuracy of the classification produced by a given threshold value was quantified using the F1-score by comparing the resulting segment classification to the 400 calibration points. Different from traditional accuracy measures, the F1-score is designed for one-class classifications [70,71] and is effective at balancing precision and recall, in

order words balancing false positives and false negatives [72]. The threshold applied to the per-segment GCC values was modified iteratively to find the threshold that produced the highest F1-score.

(3.2) For each site, once the optimal GCC threshold was found, it was applied to the segmented UAV-based orthomosaic, for that site, to produce a binary WL/OT classification map that could serve as validation for the subsequent satellite image-based workflow.

2.3.4 Step 4: Satellite Data Preparation

In order to distinguish understory vegetation from coniferous trees, a winter image (4.1) was acquired during the period when coniferous trees were the only green vegetation present in the area. Three spring images (5.1) were then acquired during periods when the wild leek had emerged and the deciduous trees canopy was still leafless. (Table 1).

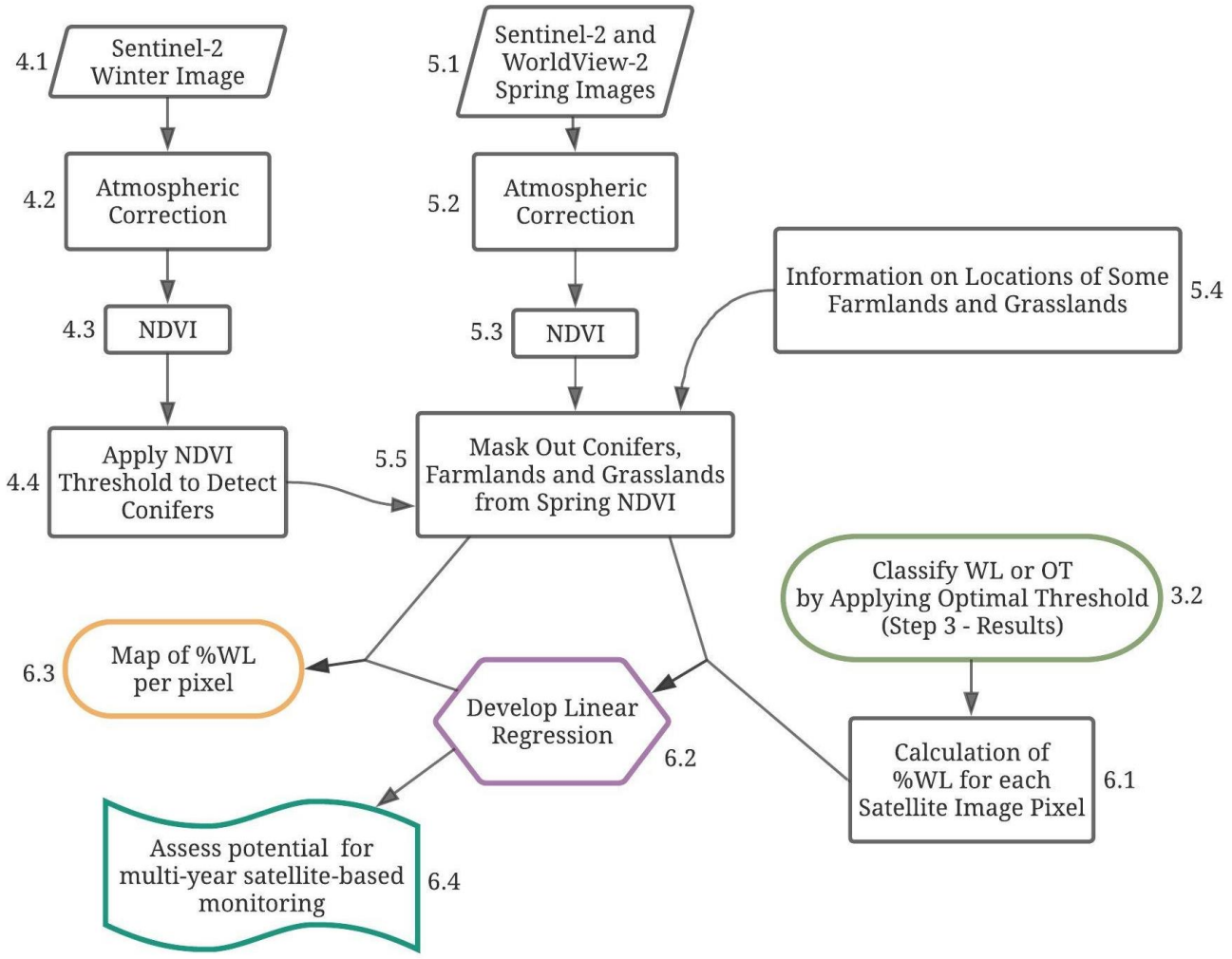

Figure 6. Workflow for processing satellite data and validating new spring image without conifers and grass.

(4.2 & 5.2) All satellite data were atmospherically corrected to surface reflectance using ATCOR in PCI Geomatica 2017, and (4.3 & 5.3) NDVI was calculated for all four images. (4.4) Visual interpretation of the winter image was then used to identify a NDVI threshold (0.06) that could be used to distinguish tree stands dominated by conifers from all other surface types in that image (Figure 7).

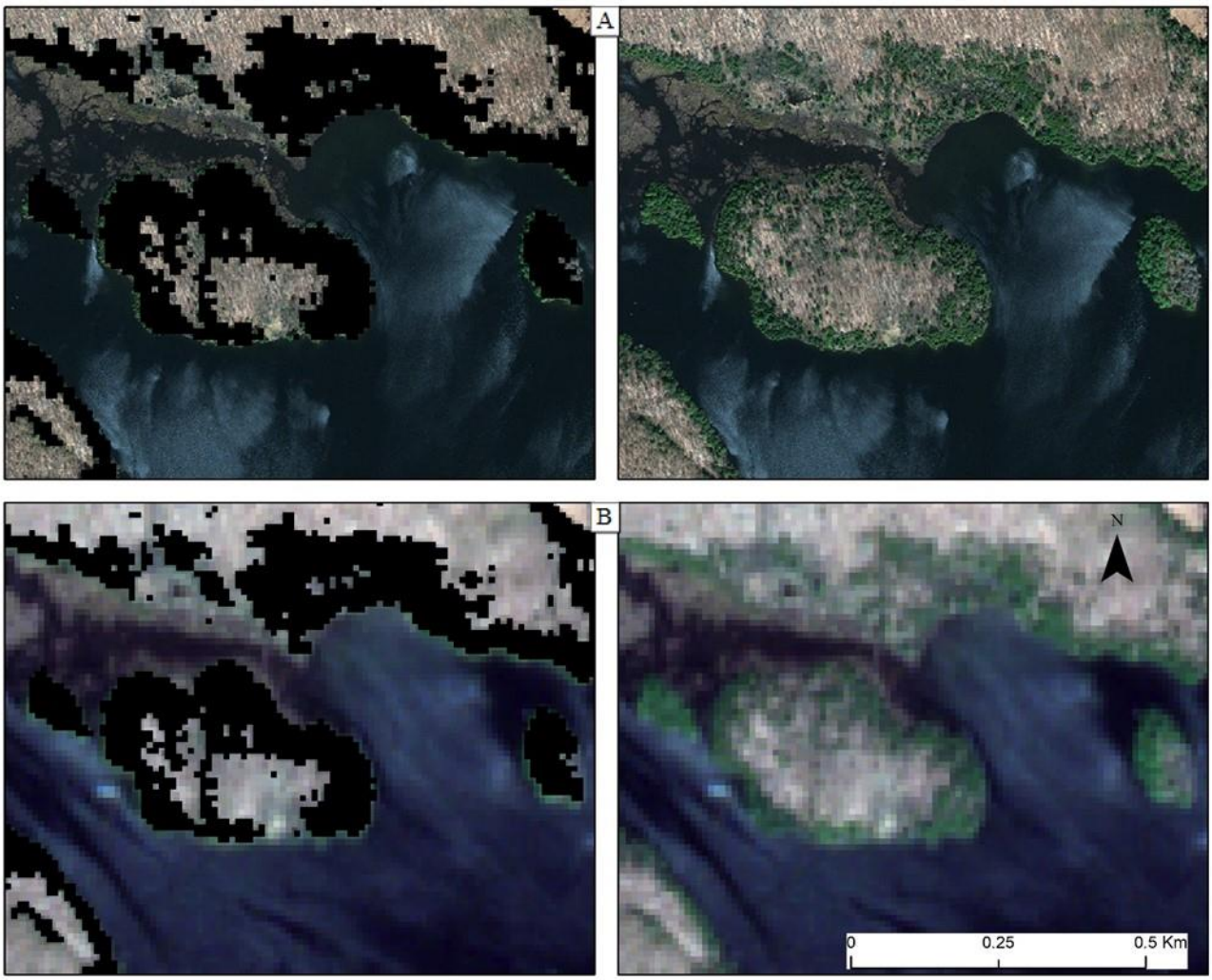

Figure 7. Pixels with NDVI > 0.06 on the Sentinel-2 winter image (left-hand side, black), were removed from the spring images for both the WorldView-2 (A) and the Sentinel-2 (B) imagery.

(5.4) Using a forest inventory shapefile provided by Quebec's Ministère des Forêts, de la Faune et des Parcs [73], large farmland and grassland patches were identified and deleted from the imagery. Not all grassy areas found at each site were highlighted in the shapefile and thus some grassy areas were not removed from the image. The forest inventory shapefile could not be used to remove conifers from the

satellite images since most of the areas containing conifers were classified as mixed forest and deleting the mixed forest areas could result in the removal of areas that contain wild leek. (5.5) The pixels with NDVI > 0.06 on the winter image, indicating conifers, were removed from all spring images. None of the pixels identified as conifers and excluded as a result were found within any of the five study sites.

2.3.5 Step 5: Satellite-based Wild Leek Mapping

With the pixel sizes of the satellite imagery used in this study (4 m^2 and 100 m^2 respectively), which are larger than all wild leek patches observed during field collection, mapping wild leek according to the percentage cover within each pixel gives more detailed information about its distribution than a binary WL/OT classification.

(6.1) To assess the strength of the relationship between satellite-based NDVI and the amount of wild leek present in an area, and thus assess the potential to map wild leek with satellite data, the classified orthomosaics from step 3 were used to quantify the percent cover of wild leek within each satellite image pixel. This process was carried out separately for the WorldView-2 and Sentinel-2 images due to their difference in pixel size (Figure 8). The classified orthomosaics, rather than field observations, were used to represent the actual amount of wild leek in each area because the very patchy nature of wild leek, with most patches covering only ~1 m^2 [7], does not allow estimation of wild leek cover from field observations for area the size of many satellite image pixels. The UAV-based wild leek maps, despite being an imperfect estimate of actual wild leek cover, were used because of their demonstrated high accuracy [7].

(6.2) Total least squares (TLS) regression was used to determine the relationship between NDVI values from the WorldView-2 spring image and the corresponding percentage wild leek (%WL) cover derived from the UAV-based orthomosaics. TLS takes observational errors from both dependent and independent variables into account when determining the regression relationship; in the present case this is more appropriate than ordinary least squares (OLS) regression, which takes only the dependent variable errors into account [74]. Second-order polynomial regression was used to determine the relationship between NDVI values from the Sentinel-2 spring images and the resampled WorldView-2 with their corresponding percentage wild leek (%WL) cover derived from the UAV-based orthomosaics. (6.3) The regression relationships were then used to map per-pixel predictions of wild leek percent cover for each satellite image.

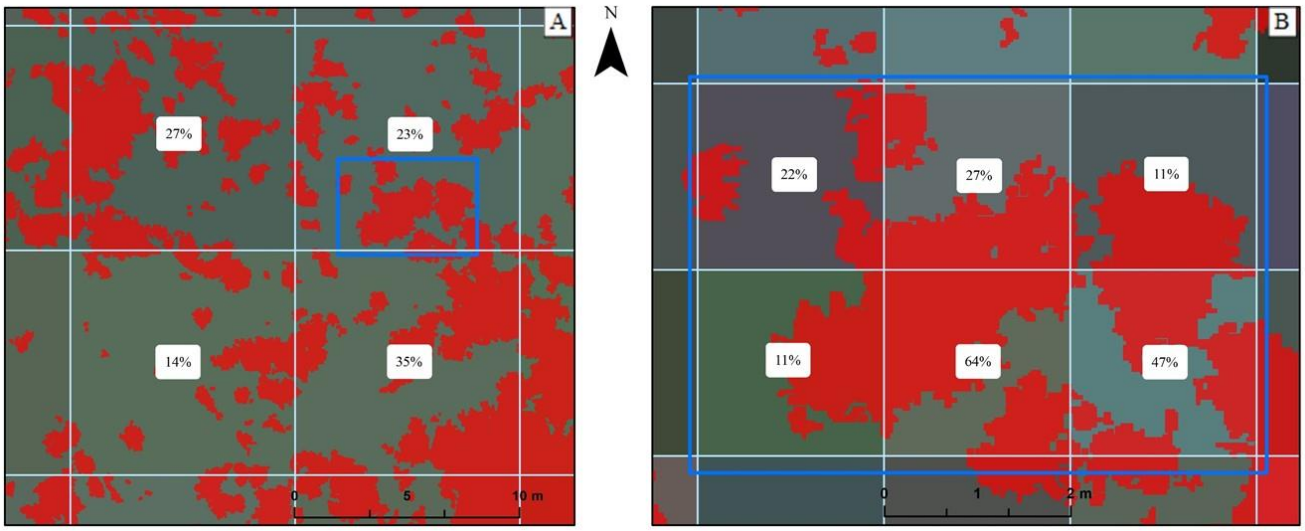

Figure 8. Percentage of wild leek per Sentinel-2 pixel (A), and per WorldView-2 pixel (B). The blue polygon, which corresponds to the same area in both images, was drawn to emphasize the difference in pixel size between the two satellites.

(6.4) To assess the potential for multi-year satellite-based wild leek monitoring without the need for repeat field and UAV data collection, two possible approaches were tested in an inter-annual analysis. a) Applying the regression relationship developed for the 2018 Sentinel-2 image directly to the 2017 Sentinel-2 image. The assumption behind this approach is that the wild leek is at the same phenological stage in both images, and that the relationship between NDVI and %WL is therefore roughly equivalent between the two images. b) Developing a new regression relationship between the %WL from the 2018 UAV-based wild leek maps and the NDVI from the 2017 Sentinel-2 imagery. The assumption behind this approach is that changes in wild leek coverage between the two years is negligible at the sites for which the field data exist, while changes in wild leek may be detected from elsewhere in the park.

2.4 Results

2.4.1 UAV-based Wild Leek Maps

By applying the optimal GCC threshold to the segmented orthomosaics for each site, wild leek was efficiently distinguished from other surface types at most sites (Figure 9-A). Very small wild leek patches were typically less accurately detected, and unmasked grass, which was present at some sites, was generally misclassified as wild leek (Figure 9-B) due to its greenness.

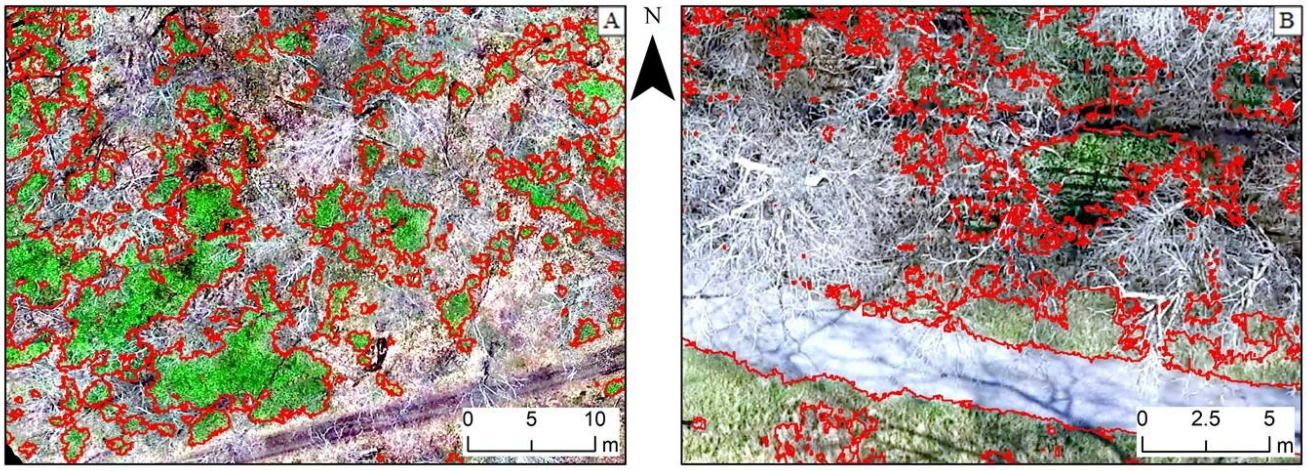

Figure 9. Sites A1 (A) and SB (B). Areas classified as wild leek are outlined as red polygons.

Since the shade of green between the grass and the wild leek is visually different (Figure 9), other methods were tested to differentiate them and eliminate the grass from the wild leek classification. Combining GCC with other vegetation indices, such as the Normalized Green-Red Difference Index (NGRDI) [75], during the classification was tested, but did not achieved improved results.

The orthomosaic from the SB site was also transformed from RGB color space to both IHS and HSV color spaces [31,50,55,76–78] as an attempt to improve the segmentation but while this did produce different segments the ability to separate grass from wild leek was not improved. To produce a quick and accurate wild leek classification for the SB site, grassy areas were therefore manually outlined and eliminated. Table 2 shows the confusion matrices and F1-scores for all five study sites.

The optimization of the GCC threshold led to a very low classification accuracy (F1 = 0.43) for the MB site, which consists of only a few small patches of wild leek on an otherwise bare or leaf-covered forest floor, and it visually misclassified large areas of decomposing leaves as wild leek. To overcome this problem, the average of the GCC threshold used for the other sites was applied instead, which resulted in no wild leek being classified within any of the four corners and the inability to calculate a F1-score. The MB site was therefore not used to calibrate the regression relationships between satellite-derived NDVI and percentage wild leek cover.

The SB site, which had one of its four corners located in a grassy area, had a very low classification accuracy (F1 = 0.46) prior to manual elimination of the grass, but an excellent accuracy afterward (F1 = 0.94). The other sites, which have bigger wild leek patches and no grassy areas, were classified well (F1-scores between 0.64 to 0.84). The optimal GCC threshold used to separate wild leek from other surface types varied between 0.336 and 0.342.

Table 2. Confusion matrices, GCC thresholds and F1-scores. [1] Optimized GCC threshold that produced highest F1-score. [2] Average value of GCC threshold of other sites. [3] The classification of the SB site was low (F1 = 0.46) prior to elimination of the grassy areas. [4] After elimination of the grassy area, the classification of wild leek at the SB site improved greatly (F1 = 0.94).

Sites	Classification				GCC threshold	F1-score
	Reference Data	WL	OT	Total		
A1	**WL**	29	19	48	0.336	0.64
	OT	14	338	352		
	Total	43	357	400		
A2	**WL**	44	12	56	0.336	0.72
	OT	22	322	344		
	Total	66	334	400		
A3	**WL**	66	9	75	0.336	0.84
	OT	17	308	325		
	Total	83	317	400		
MB [1]	**WL**	3	2	5	0.321	0.43
	OT	6	389	395		
	Total	9	391	400		
MB [2]	**WL**	0	5	5	0.338	N/A
	OT	0	395	395		
	Total	0	400	400		
SB [3]	**WL**	29	3	32	0.342	0.46
	OT	66	302	368		
	Total	95	305	400		
SB [4]	**WL**	29	3	32	0.342	0.94
	OT	1	267	268		
	Total	30	270	300		

Figure 10 shows the relationship between the F1-scores for the 5 sites as a function of the GCC threshold values. The relationship proves the existence of the optimal GCC threshold and its expected F1-score for each site.

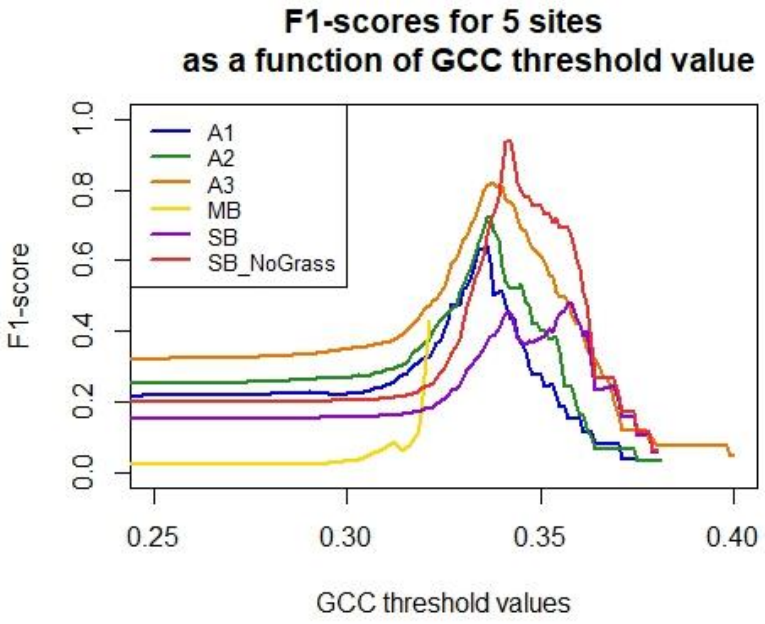

Figure 10. F1-scores as a function of the GCC threshold values.

2.4.2 Satellite-based Wild Leek Detection

The linear model predicting the percentage of wild leek (%WL) from satellite-based NDVI has a good fit when based on the Sentinel-2 imagery from 2018 (R^2 = 0.58; RMSE = 10.32; p-value = < 2.2e-16) (Figure 11). Pixels with %WL equal to zero were kept for all regression calculations but negative %WL values predicted from the regression equation were converted to zeros before the calculation of all R^2 and RMSE values.

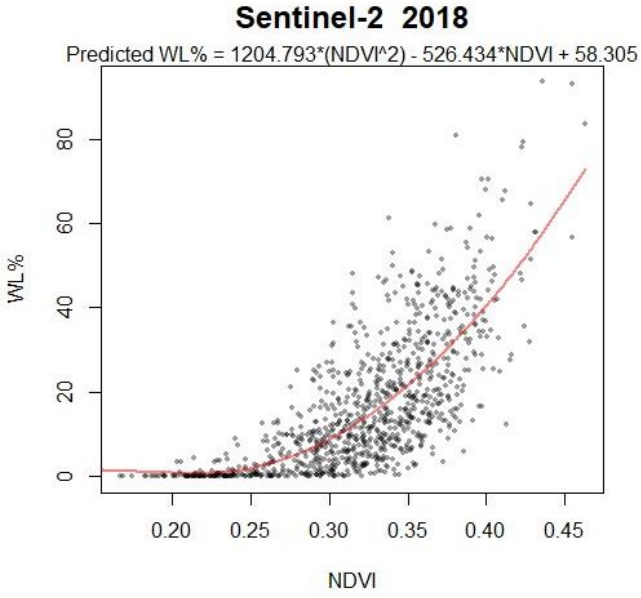

Figure 11. Regression based on the Sentinel-2 image and the UAV-based wild leek maps from 2018.

While a relationship is also clearly present when using the 2018 WorldView-2 imagery, it is markedly noisier than the one for Sentinel-2 (R^2 = 0.15; RMSE = 37.64; p-value: < 2.2e-16) (Figure 12). To assess if this is due to the smaller pixel size of WorldView-2 and the resulting greater influence of imperfect relative geolocation between the satellite image and the UAV-based wild leek map, the WorldView-2 imagery was resampled to 10 meters to match the pixel size of Sentinel-2 imagery. This tightened the relationship substantially (R^2 = 0.32; RMSE = 13.06; p-value: < 2.2e-16) (Figure 13), although it remains noisier than the one obtained from Sentinel-2. The scale effect of the modifiable areal unit problem (MAUP), is the primary reason for how WorldView-2 has initially a worse fit than Sentinel-2 and for how WorldView-2 has a better fit when resampled to 10 meters. Besides the aggregation, which is in this case the primary cause of the MAUP effect, imperfect georeferenced also contributes for the coarser fit of WorldView-2 [79,80].

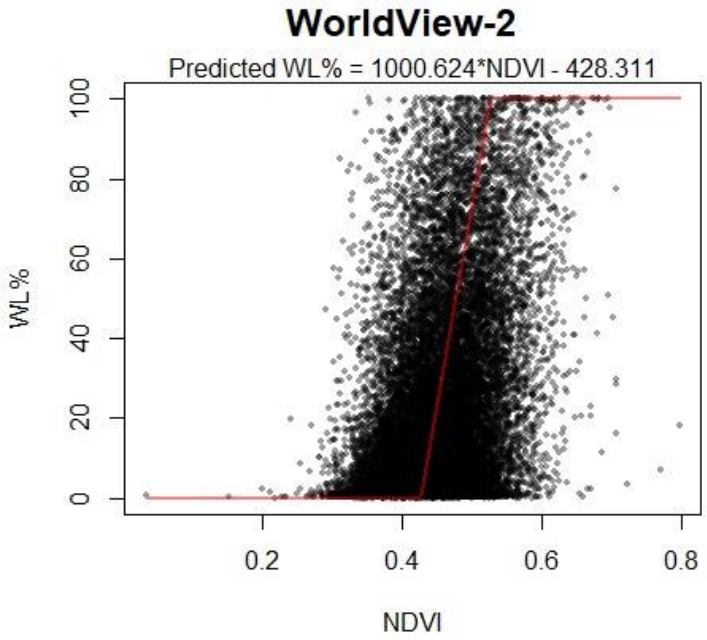

Figure 12. Regression based on the WorldView-2 image and the UAV-based wild leek maps from 2018.

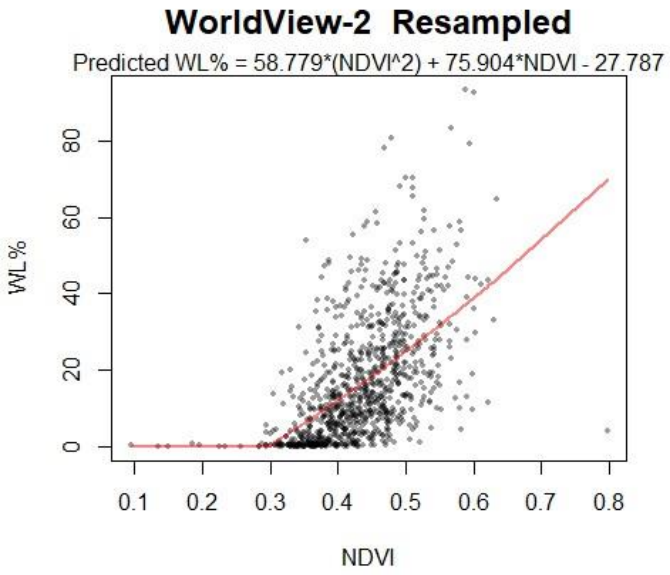

Figure 13. Regression based on the resampled WorldView-2 image and the UAV-based wild leek maps from 2018.

2.4.3 Inter-annual Analysis

Applying the polynomial regression equation developed for the 2018 Sentinel-2 image directly to the 2017 Sentinel-2 image produced relatively larger errors in %WL prediction (R^2 = 0.33; RMSE = 16.97; p-value: < 2.2e-16), and it is clear from a comparison of this regression line with the %WL values and the NDVI values from the 2017 Sentinel-2 image that direct use of a regression relationship developed in one year to imagery from another year is likely to produce biased %WL predictions (Figure 14).

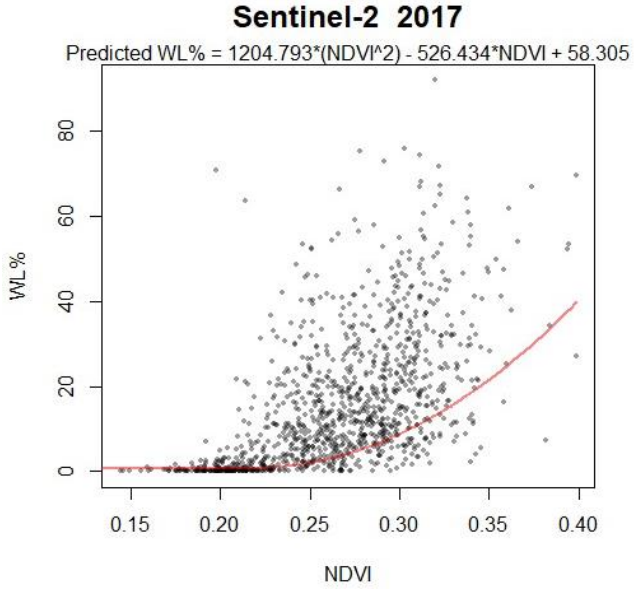

Figure 14. Regression based on the Sentinel-2 image from 2018, compared with the %WL and NDVI values from the Sentinel-2 image from 2017.

Developing a new regression relationship using the Sentinel-2 image from 2017 and the wild leek maps from 2018 also provided relatively larger errors in %WL prediction (R^2 = 0.33; RMSE = 12.84; p-value: < 2.2e-16) (Figure 15).

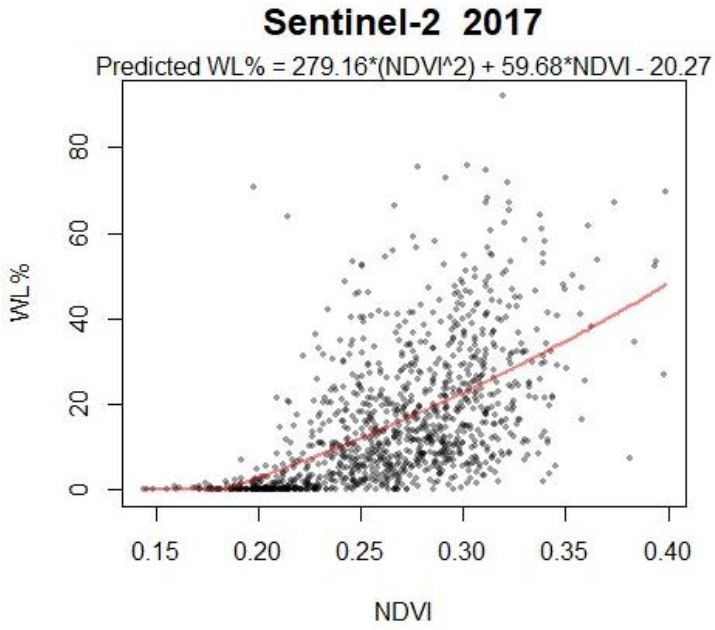

Figure 15. Regression based on the Sentinel-2 from 2017, and the UAV-based wild leek maps from 2018.

2.4.4 Percentage of Wild Leek Coverage maps

The regression equations developed for the Sentinel-2 and WorldView-2 images from 2018 were used to create maps of percent wild leek cover. Figure 16 shows the wild leek map for all of Gatineau Park based on the Sentinel-2 imagery, and Figure 17 shows the map based on the full extent of the WorldView-2 imagery, which covers only the southern portion of the park.

Figure 18 shows a comparison the maps produced from Sentinel-2 and WorldView-2 imagery, for an area with abundant wild leek. Figure 19 shows a comparison between the wild leek prediction for Sentinel-2 and the resampled WorldView-2 imagery (F1-score = 0.18).

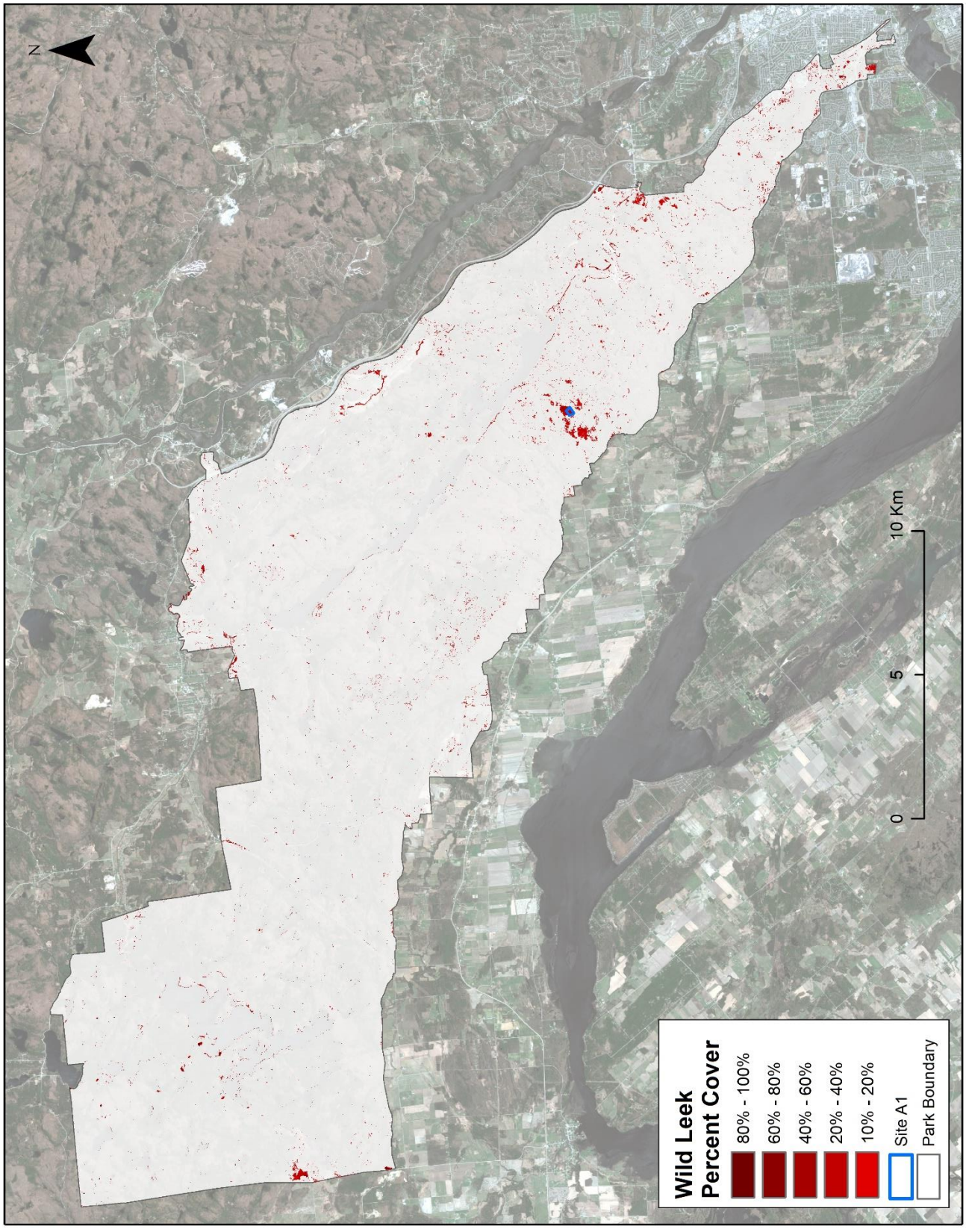

Figure 16. Percentage of wild leek coverage map for Sentinel-2 imagery from May 9, 2018.

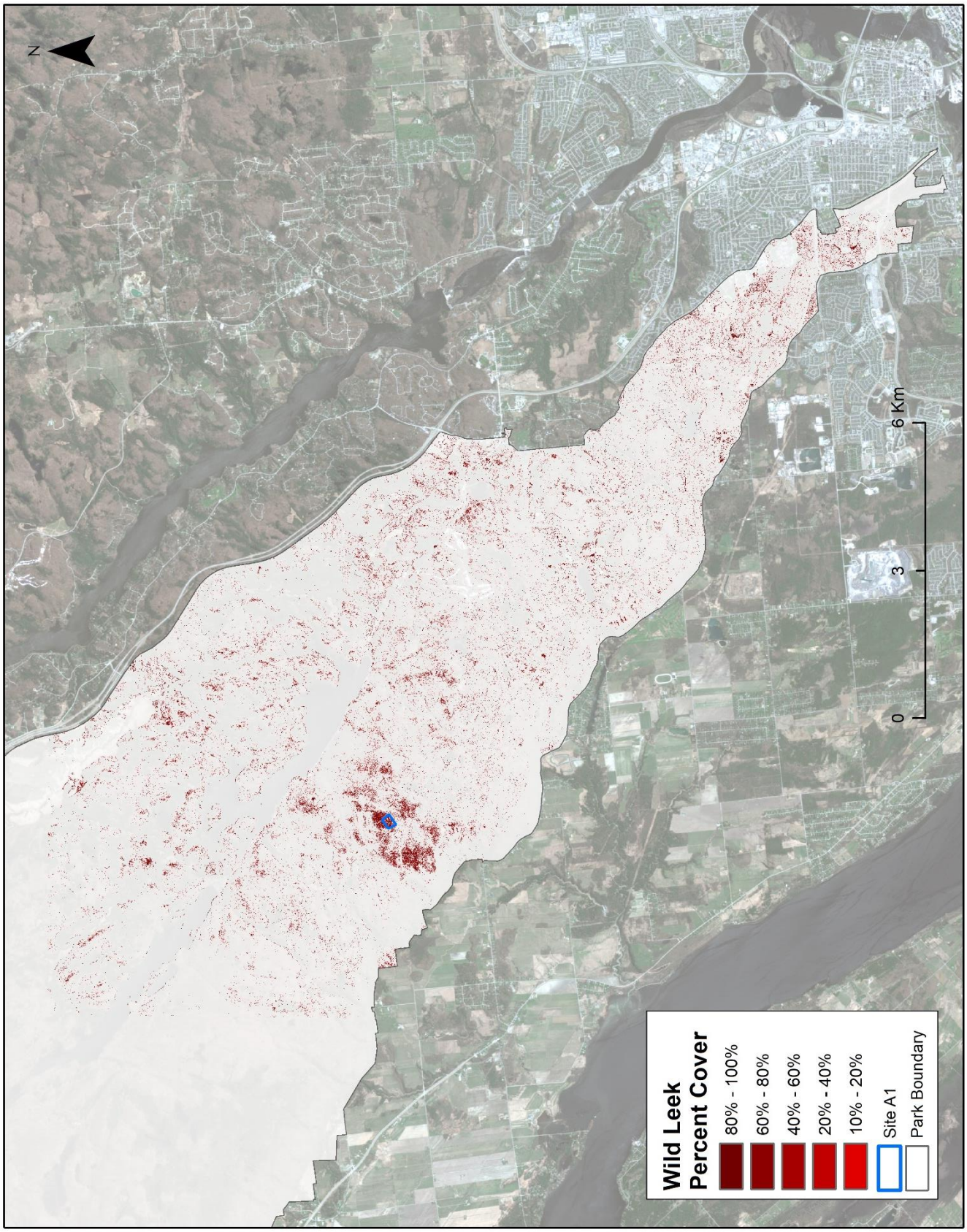

Figure 17. Percentage of wild leek coverage map for WorldView-2 imagery from May 6, 2018.

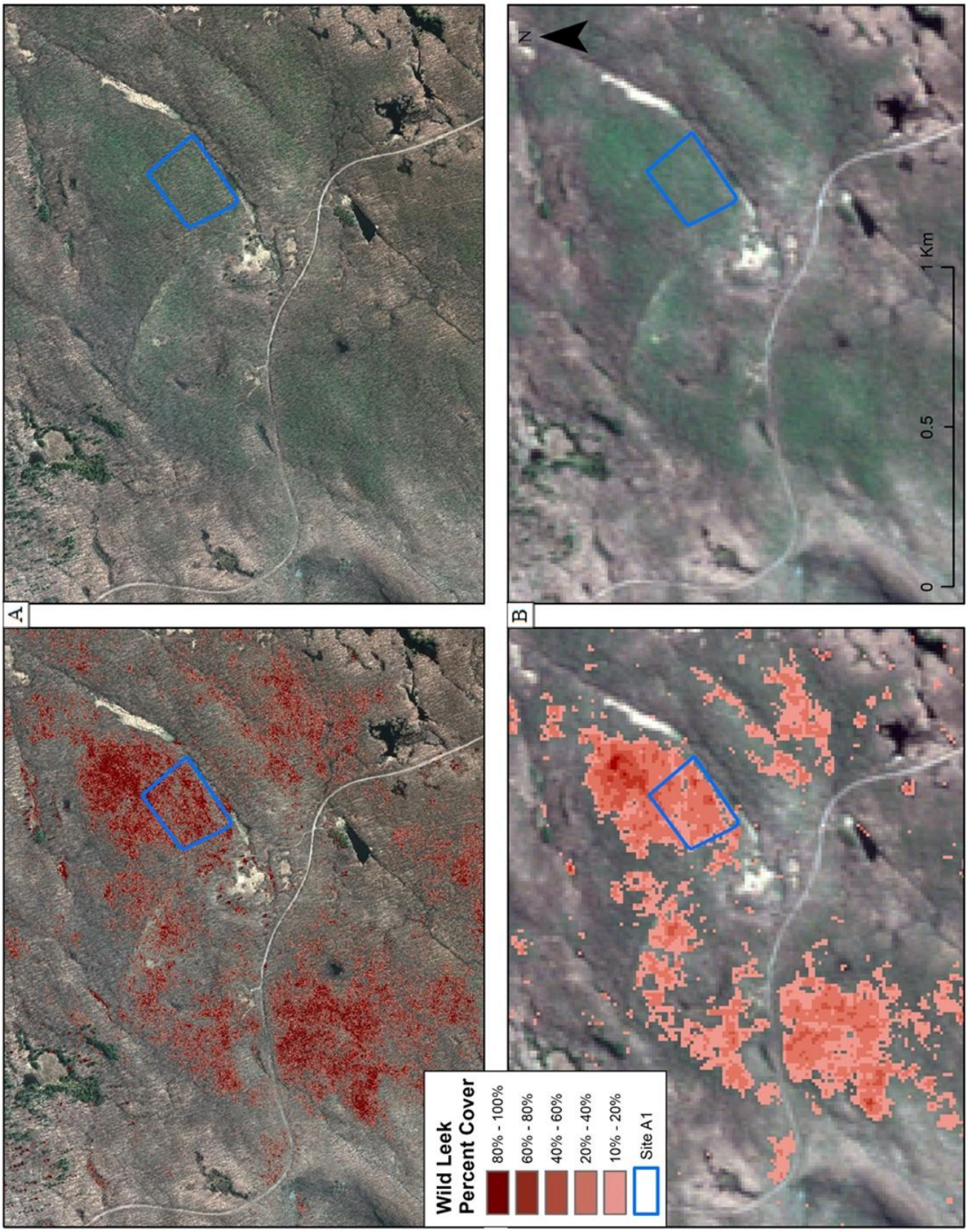

Figure 18. Comparison between WorldView-2 (A) and Sentinel-2 (B) coverage maps.

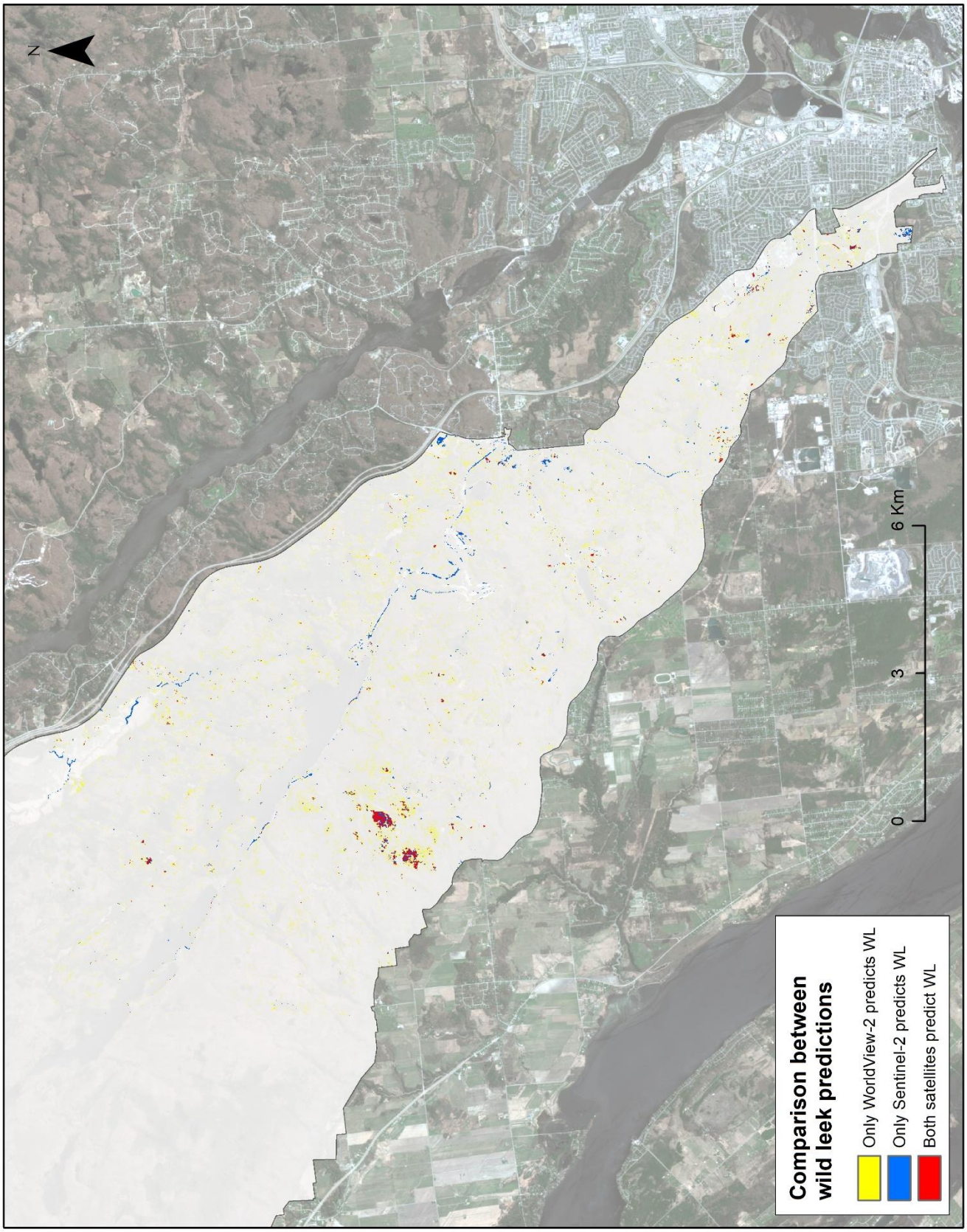

Figure 19. Comparison between the wild leek predictions for Sentinel-2 and WorldView-2

2.5 Discussion

While providing some opportunities for mapping understory vegetation, near-surface remote sensing based on UAVs acquires high-resolution imagery at the cost of covering small spatial extents [7], and it is therefore unsuited on its own for monitoring vegetation across sites the size of many protected areas, including Gatineau Park. Mapping wild leek by using UAV video to calibrate a regression model for satellite imagery provides an option for mapping and monitoring wild leek in all of Gatineau Park, producing maps similar to those based on field observations [69] but with complete spatial coverage. However, the comparability between the UAV image and the satellite image might be influenced by unwanted variability, such as scene illumination in imagery due to shadows and clouds. Therefore, a careful interpretation of the output is important in order to avoid biased results. Nevertheless, the method is fast and easily repeatable when compared to field-based methods, and in addition to detecting the presence/absence of wild leek it also produces a measure of density, quantified as percent ground cover.

The high-resolution maps based on ground and UAV data had high overall accuracy (F1-scores between 0.64 to 0.84), and importantly they were able to detect the differences between the sites, e.g. while dense wild leek was correctly found at sites A1, A2 and A3, once the corrected GCC threshold was applied no wild leek patches was detected within the four corners at the MB site, which indeed has only very few, small and sparse patches of wild leek. The use of a simple greenness threshold to identify wild leek worked well for those sites, but failed at the SB site due to the substantial amount of grass present there. However, manual removal of grass from the wild leek map of the SB site was quick and easy, and resulted in a very accurate wild leek map for this site (F1 = 0.94). The optimal GCC threshold is reasonably constant when applied to sites with similar environments (e.g. A1, A2 and A3), but changes considerably when applied across different sites, such as SB (greater prevalence of other understory vegetation) and MB (thick cover of decomposing leaves, and negligible amounts of wild leek). Thus, the effectiveness of using a constant GCC threshold value across space was shown to be impracticable [7].

The relationship between percent wild leek cover derived from UAV video and NDVI from the Sentinel-2 image acquired in 2018 (two days after the UAV flights) was strong, and allowed the percent wild leek cover to be predicted from the satellite imagery with an RMSE of 10.32. The WorldView-2 image (acquired the day before the UAV-flight) showed a much noisier relationship (RMSE = 37.64), which was partly improved by resampling to match the 10 m spatial resolution of the Sentinel-2 imagery (RMSE = 13.06), due to MAUP scale effect. These two sources of satellite imagery

allowed production of similar wild leek maps (Figure 16 and Figure 17) that, based on experience from field and visual inspection of the imagery, provide good descriptions of the actual distribution of wild leek at the studied sites.

The comparison between the wild leek prediction maps for Sentinel-2 and the resampled WorldView-2 images (Figure 19) had low accuracy (F1 = 0.18) due to misclassification of the remaining coniferous pixels as wild leek. Figure 20 shows that the NDVI threshold (0.06) applied on the Sentinel-2 winter image to remove coniferous pixels from the spring images worked well on the Sentinel-2 image but not so well on the WorldView-2 image. As we can see on Figure 20-A, there are many red pixels (%WL prediction), in areas where clearly there are coniferous trees. The resampled WorldView-2 image had more than four times more pixels misclassified as wild leek than the Sentinel-2 image, which is the main reason for the low F1-score It is expected that a winter satellite image, with higher spatial resolution, could have been able to remove the coniferous pixels present in the WorldView-2 image better than the winter Sentinel-2 image. The selection of the "winter" image is critical to eliminate coniferous successfully.

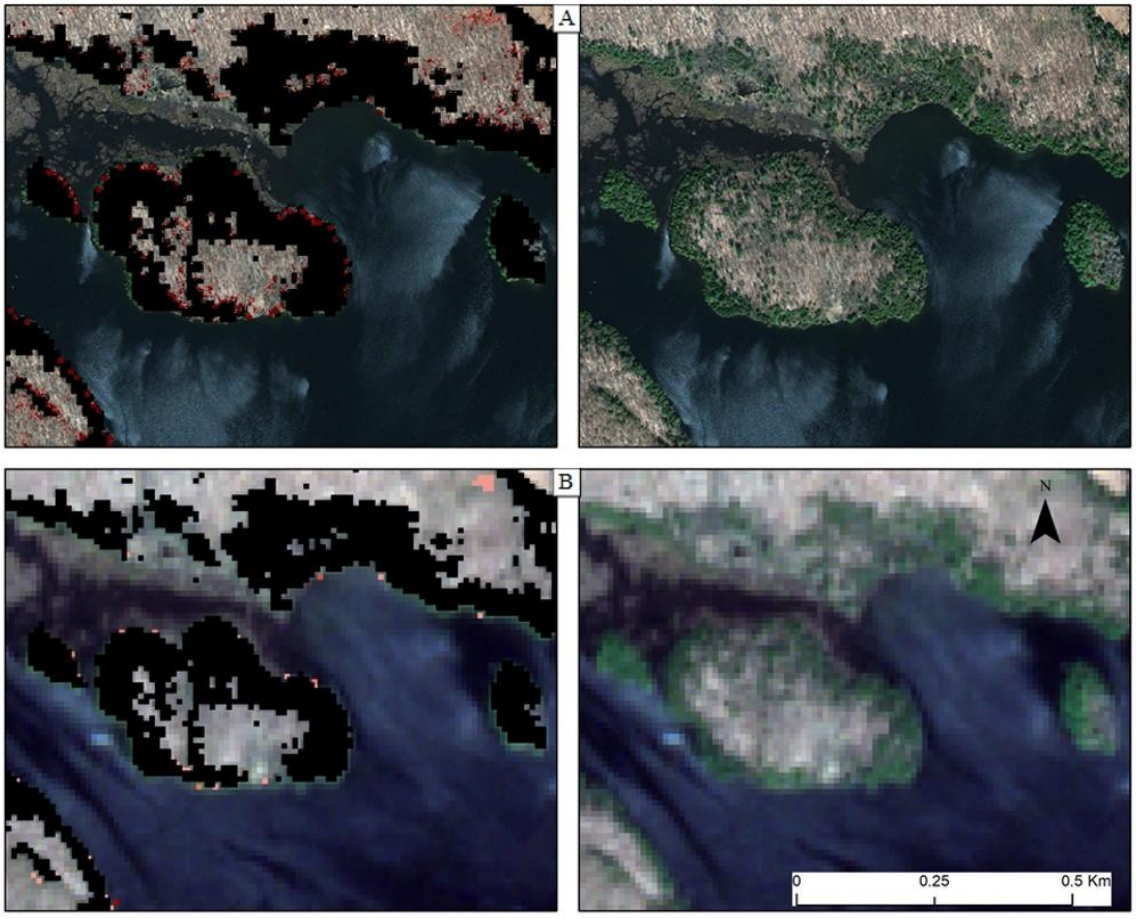

Figure 20. Remaining conifers pixels were misclassified as wild leek on both images, WorldView-2 (A) and Sentinel-2 (B).

For the inter-annual analysis, the relationship between NDVI from the 2017 Sentinel-2 image and the percent wild leek cover from 2018 produced a similar error in %WL prediction when a new regression was developed (RMSE = 12.84) as when the regression line calibrated with the 2018 image was applied (RMSE = 16.97). It is not surprising that the relationship between UAV-based wild leek map acquired in 2018 is better with the 2018 Sentinel-2 image, since the phenological development of wild leek is more likely to be similar to the image that was acquired the same year than to an image that was acquired in a different year from the field and UAV data. It is expected that the higher RMSE obtained with the 2017 Sentinel-2 image is more related to the timing difference on the stage of wild leek development between the fieldwork and satellite date than with the actual change of wild leek coverage. This suggests that if possible, all data should be acquired in the same year, and at the same time. However, for monitoring purposes, the relatively small increase in RMSE when applying a linear model to imagery collected at a similar time but in a different year suggests that the NDVI-%WL relationship can be stable between years, and that wild leek distribution therefore can be monitored without the need for coincident field and UAV data collection.

The potential to use satellite imagery for monitoring wild leek, in addition to producing a map of its current distribution, thus depends on a) the cost of producing each map update, and b) the accuracy with which change can be detected between subsequent maps.

2.5.1 Limitations

The principal limitation of the method is that it depends on the existence of cloud-free satellite imagery from the relatively short (~5 week) period during which green wild leek is visible through the leafless canopy. With Sentinel-2 data, and depending on local cloud climatology, this typically limits its application to contexts in which periods of 2-3 years between wild leek map updates would be acceptable. However, this limitation is likely to become less important over the coming decade as multiple satellite constellations (e.g. from Planet, DigitalGlobe) will provide daily global imaging capability at ~ 5m spatial resolution, covering the visible and near-infrared wavelengths.

Despite the generally high accuracy of the UAV-based wild leek maps, an efficient approach that distinguishes grass from wild leek in an automated fashion is needed. None of our attempts to separate grass from wild leek were successful, and a method to overcome this problem is important to eliminate grass patches from the wild leek maps produced from UAV data. It is likely that a sensor with additional spectral resolution would be capable of automatically separating those two types of vegetation and also better discriminate wild leek from other forest floor species [7].

In a future application of the method developed and presented in this study, we suggest obtaining ground and UAV data from sites with a greater range of wild leek coverage and forest floor background, to ensure that the full range of environments found in Gatineau Park are better represented in the data points used to calibrate the NDVI-wild leek regression relationship. We also recommend that all the data should be collected in the same year, although the one-year difference between field/UAV data and satellite imagery tested here did not increase predictions errors greatly. Whether this increase in prediction errors is acceptable given that the approach allows updating wild leek maps for a large area without conducting additional fieldwork will depend on management context. Using this methodology, the monitoring frequency of species at risk in Gatineau Park, including wild leek, that is currently 5 years [65,66], could decrease to every 2 to 3 years. This approach could thus simultaneously reduce the cost and increase the spatial extent and frequency of monitoring, compared to current labour- and time-intensive methods that are based on human field observations.

3 Conclusion

Using ground photos, UAV video and satellite imagery collected during the short period of the year when wild leek is visible through the leafless canopy, this study demonstrated the ability to map wild leek across the full ~361 km^2 Gatineau Park, Canada. UAV-based wild leek maps were produced at a low cost for small areal extents, and used to calibrate regression relationships between satellite-derived NDVI and percentage wild leek cover. Despite the two different vegetation indexes used to detected wild leek, GCC and NDVI were both able to provide comparable high accuracy results. When applied to Sentinel-2 or WorldView-2 satellite imagery, percentage wild leek cover was predicted with RMSE values smaller than 20, and visual assessment of the resulting wild leek maps suggested they provide an accurate portrayal of wild leek distribution in the park. Most of the areas where there was misclassification of wild leek belong to coniferous trees that were not perfectly excluded from the spring images. Application of UAV data or calibrated regression relationships to satellite imagery from a different year only slightly increased wild leek cover prediction errors, suggesting strong potential for wild leek monitoring with this approach. The data acquisition and processing workflow, outlined in detail in this study, is an effective method to map wild leek in Gatineau Park, though removal of grassy areas is required for improved automation.

4 References

1. Bernatchez, A.; Lapointe, L. Cooler temperatures favour growth of wild leek (*Allium tricoccum*), a deciduous forest spring ephemeral. *Botany* **2012**, *90*, 1125–1132, doi:10.1139/b2012-089.
2. Nantel, P.; Gagnon, D.; Nault, A. Population viability analysis of American ginseng and wild leek harvested in stochastic environments. *Conserv. Biol.* **1996**, *10*, 608–621, doi:10.1046/j.1523-1739.1996.10020608.x.
3. Nault, A.; Gagnon, D. Ramet Demography of Allium Tricoccum, A Spring Ephemeral, Perennial Forest Herb. Published by: British Ecological Society Stable URL: http://www.jstor.org/stable/2261228. *J. Ecol.* **1993**, *81*, 101-119.
4. Nault, A.; Gagnon, D. Seasonal Biomass and Nutrient Allocation patterns in Wild Leek (Allium tricoccum Ait.), a Spring Geophyte. Source: Bulletin of the Torrey Botanical Club, Vol. 115, No. 1 (Jan . - Mar ., 1988), pp . 45-5. **1988**, *115*, 45–54.
5. Dion, P.P.; Bussières, J.; Lapointe, L. Sustainable leaf harvesting and effects of plant density on wild leek cultivation plots and natural stands in Southern Quebec, Canada. *Agrofor. Syst.* **2016**, *90*, 979–995, doi:10.1007/s10457-015-9878-7.
6. Regulation respecting threatened or vulnerable plant species and their habitats. Available online: http://legisquebec.gouv.qc.ca/en/ShowDoc/cr/E-12.01,%20r.%203 (accessed on 12 December 2017)..
7. Leduc, M.; Knudby, A.J. Mapping Wild Leek through the Forest Canopy Using a UAV. **2018**, 1–15, doi:10.3390/rs10010070.
8. Shouse, M.; Liang, L.; Fei, S. Identification of understory invasive exotic plants with remote sensing: In urban forests. *Int. J. Appl. Earth Obs. Geoinf.* **2012**, *21*, 525–534, doi:10.1016/j.jag.2012.07.010.
9. Wilfong, B.N.; Gorchov, D.L.; Henry, M.C. Detecting an Invasive Shrub in Deciduous Forest Understories Using Remote Sensing. *Weed Sci.* **2009**, *57*, 512–520, doi:10.1614/WS-09-012.1.
10. Tuanmu, M.N.; Viña, A.; Bearer, S.; Xu, W.; Ouyang, Z.; Zhang, H.; Liu, J. Mapping understory vegetation using phenological characteristics derived from remotely sensed data. *Remote Sens. Environ.* **2010**, *114*, 1833–1844, doi:10.1016/j.rse.2010.03.008.
11. Becker, R.H.; Zmijewski, K.A.; Crail, T. Seeing the forest for the invasives: Mapping buckthorn in the Oak Openings. *Biol. Invasions* **2013**, *15*, 315–326, doi:10.1007/s10530-012-0288-8.

12. Parcs Québec The Environmental Indicators Monitoring Program. Available online: https://www.sepaq. com/dotAsset/6ea4e70c-0210-4231-819f-0934a3b4f1d4.pdf (accessed on 15 August 2018).
13. Vasseur, L.; Gagnon, D. Survival and Growth of Allium-Tricoccum Ait Transplants in Different Habitats. *Biol. Conserv.* **1994**, *68*, 107–114, doi:10.1016/0006-3207(94)90340-9.
14. Wing, B.M.; Ritchie, M.W.; Boston, K.; Cohen, W.B.; Gitelman, A.; Olsen, M.J. Prediction of understory vegetation cover with airborne lidar in an interior ponderosa pine forest. *Remote Sens. Environ.* **2012**, *124*, 730–741, doi:10.1016/j.rse.2012.06.024.
15. Wilson, B.A.; Ference, C.G. The influence of canopy closure on the detection of understory indicator plants in kananaskis country. *Can. J. Remote Sens.* **2001**, *27*, 207–215, doi:10.1080/07038992.2001.10854937.
16. Tremblay, N.O.; Larocque, G.R. Seasonal Dynamics of Understory Vegetation in Four Eastern Canadian Forest Types Author (s): Nicolas O . Tremblay and Guy R . Larocque Published by : The University of Chicago Press Stable URL : https://www.jstor.org/stable/10.1086/319582 SEASONAL DYNAM. **2001**, *162*, 271–286.
17. Lapointe, L. How phenology influences physiology in deciduous forest spring ephemerals. *Physiol. Plant.* **2001**, *113*, 151–157, doi:10.1034/j.1399-3054.2001.1130201.x.
18. Dion, P.-P.; Bussières, J.; Lapointe, L. Late canopy closure delays senescence and promotes growth of the spring ephemeral wild leek (*Allium tricoccum*). *Botany* **2017**, *95*, 457–467, doi:10.1139/cjb-2016-0317.
19. Davis, J.M.; Greenfield, J. Cultivating Ramps : Wild Leeks of Appalachia. **2002**, 449–452.
20. Edgar, B.; Brubaker, H.; Tuminelli, K. Plugging the Leak on Wild Leeks : The Threat of Over-harvesting Wild Leek Populations in Northern New York. **2012**. Available online: http://www.stlawu.edu/sites/default/ files/resource/wild_leek_conservation.pdf (accessed on 20 January 2018).
21. Espèce Vulnérable Au Québec. Available online: http://www.mddelcc.gouv.qc.ca/biodiversite/ especes/ail/index.htm (accessed on 05 November 2018).
22. Rock, J.H.; Beckage, B.; Gross, L.J. Population recovery following differential harvesting of Allium tricoccum Ait. in the southern Appalachians. *Biol. Conserv.* **2004**, *116*, 227–234, doi:10.1016/S0006-3207(03)00193-9.
23. Jones, A.G. A Study of Wild Leek , and the Recognition of Allium burdickii (Liliaceae) Author (s): Almut G . Jones Published by : American Society of Plant Taxonomists Stable URL : http://www.jstor.org/stable/2418663. *Syst. Bot.* **1979**, *4*, 29–43.

24. Singh, K.K.; Davis, A.J.; Meentemeyer, R.K. Detecting understory plant invasion in urban forests using LiDAR. *Int. J. Appl. Earth Obs. Geoinf.* **2015**, *38*, 267–279, doi:10.1016/j.jag.2015.01.012.
25. Conservation of Gatineau Park Gatineau. Available online: http://ncc-ccn.gc.ca/places/conservation-at-gatineau-park (accessed on 05 November 2018).
26. Pasher, J.; King, D.J. Mapping dead wood distribution in a temperate hardwood forest using high resolution airborne imagery. *For. Ecol. Manage.* **2009**, *258*, 1536–1548, doi:10.1016/j.foreco.2009.07.009.
27. Burgan, R.E.; Hartford, R.A. Monitoring vegetation greenness with satellite data. *For. Serv.* **1993**, 13.
28. Resasco, J.; Hale, A.N.; Henry, M.C.; Gorchov, D.L. Detecting an invasive shrub in a deciduous forest understory using latefall Landsat sensor imagery. *Int. J. Remote Sens.* **2007**, *28*, 3739–3745, doi:10.1080/01431160701373721.
29. Rango, A.; Laliberte, A.S.; Herrick, J.E.; Winters, C.; Havstad, K.; Steele, C.; Browning, D. Unmanned aerial vehicle-based remote sensing for rangeland assessment, monitoring, and management. *J. Appl. Remote Sens.* **2009**, *3*, 033542, doi:10.1117/1.3216822.
30. Díaz-Varela, R.A.; de la Rosa, R.; León, L.; Zarco-Tejada, P.J. High-resolution airborne UAV imagery to assess olive tree crown parameters using 3D photo reconstruction: Application in breeding trials. *Remote Sens.* **2015**, *7*, 4213–4232, doi:10.3390/rs70404213.
31. Laliberte, A.S.; Herrick, J.E.; Rango, A.; Winters, C. Acquisition, Orthorectification, and Object-based Classification of Unmanned Aerial Vehicle (UAV) Imagery for Rangeland Monitoring. *Photogramm. Eng. Remote Sens.* **2010**, *76*, 661–672, doi:10.14358/PERS.76.6.661.
32. Turner, D.; Lucieer, A.; Watson, C. An automated technique for generating georectified mosaics from ultra-high resolution Unmanned Aerial Vehicle (UAV) imagery, based on Structure from Motion (SFM) point clouds. *Remote Sens.* **2012**, *4*, 1392–1410, doi:10.3390/rs4051392.
33. Wang, H.; Zhao, Y.; Pu, R.; Zhang, Z. Mapping Robinia Pseudoacacia Forest Health Conditions by Using Combined Spectral, Spatial, and Textural Information Extracted from IKONOS Imagery and Random Forest Classifier. **2015**, 9020–9044, doi:10.3390/rs70709020.
34. Müllerová, J.; Bartaloš, T.; Brůna, J.; Dvořák, P.; Vítková, M. Unmanned aircraft in nature conservation: an example from plant invasions. *Int. J. Remote Sens.* **2017**, *38*, 2177–2198, doi:10.1080/01431161.2016.1275059.
35. Laliberte, A.S.; Rango, A. Incorporation of texture, intensity, hue, and saturation for rangeland monitoring with unmanned aircraft imagery. *GEOBIA Proc.* **2008**, *XXXVII*, 4/C1.

36. Torres-Sánchez, J.; López-Granados, F.; De Castro, A.I.; Peña-Barragán, J.M. Configuration and Specifications of an Unmanned Aerial Vehicle (UAV) for Early Site Specific Weed Management. *PLoS One* **2013**, *8*, doi:10.1371/journal.pone.0058210.
37. Mafanya, M.; Tsele, P.; Botai, J.; Manyama, P.; Swart, B.; Monate, T. Evaluating pixel and object based image classification techniques for mapping plant invasions from UAV derived aerial imagery: Harrisia pomanensis as a case study. *ISPRS J. Photogramm. Remote Sens.* **2017**, *129*, 1–11, doi:10.1016/j.isprsjprs.2017.04.009.
38. Micheletti, N.; Chandler, J.H.; Lane, S.N. Investigating the geomorphological potential of freely available and accessible structure-from-motion photogrammetry using a smartphone. *Earth Surf. Process. Landforms* **2015**, *40*, 473–486, doi:10.1002/esp.3648.
39. Jensen, J.L.R.; Mathews, A.J. Assessment of image-based point cloud products to generate a bare earth surface and estimate canopy heights in a woodland ecosystem. *Remote Sens.* **2016**, *8*, doi:10.3390/rs8010050.
40. Westoby, M.J.; Brasington, J.; Glasser, N.F.; Hambrey, M.J.; Reynolds, J.M. "Structure-from-Motion" photogrammetry: A low-cost, effective tool for geoscience applications. *Geomorphology* **2012**, *179*, 300–314, doi:10.1016/j.geomorph.2012.08.021.
41. Berra, E.F.; Gaulton, R.; Barr, S. Use of a digital camera onboard a UAV to monitor spring phenology at individual tree level. *Int. Geosci. Remote Sens. Symp.* **2016**, *2016–Novem*, 3496–3499, doi:10.1109/IGARSS.2016.7729904.
42. Matiu, M.; Bothmann, L.; Steinbrecher, R.; Menzel, A. Monitoring succession after a non-cleared windthrow in a Norway spruce mountain forest using webcam, satellite vegetation indices and turbulent CO2exchange. *Agric. For. Meteorol.* **2017**, *244–245*, 72–81, doi:10.1016/j.agrformet.2017.05.020.
43. Saitoh, T.M.; Nagai, S.; Saigusa, N.; Kobayashi, H.; Suzuki, R.; Nasahara, K.N.; Muraoka, H. Assessing the use of camera-based indices for characterizing canopy phenology in relation to gross primary production in a deciduous broad-leaved and an evergreen coniferous forest in Japan. *Ecol. Inform.* **2012**, *11*, 45–54, doi:10.1016/j.ecoinf.2012.05.001.
44. Toomey, M.; Friedl, M.A.; Frolking, S.; Hufkens, K.; Klosterman, S.; Sonnentag, O.; Baldocchi, D.D.; Bernacchi, C.J.; Biraud, S.C.; Bohrer, G.; Brzostek, E.; Burns, S.P.; Coursolle, C.; Hollinger, D.Y.; Margolis, H.A.; McCaughey, H.; Monson, R.K.; Munger, J.W.; Pallardy, S.; Phillips, R.P.; Torn, M.S.; Wharton, S.; Zeri, M.; Richardson, A.D. Greenness indices from digital cameras predict the timing and seasonal dynamics of canopy-scale photosynthesis. *Ecol. Appl.* **2015**, *25*, 99–115, doi:10.1890/14-0005.1.

45. Feng, Q.; Liu, J.; Gong, J. UAV Remote sensing for urban vegetation mapping using random forest and texture analysis. *Remote Sens.* **2015**, *7*, 1074–1094, doi:10.3390/rs70101074.
46. Laliberte, A.S.; Rango, A. Texture and scale in object-based analysis of subdecimeter resolution unmanned aerial vehicle (UAV) imagery. *IEEE Trans. Geosci. Remote Sens.* **2009**, *47*, 1–10, doi:10.1109/TGRS.2008.2009355.
47. Alvarez-Taboada, F.; Paredes, C.; Julián-Pelaz, J. Mapping of the invasive species Hakea sericea using Unmanned Aerial Vehicle (UAV) and worldview-2 imagery and an object-oriented approach. *Remote Sens.* **2017**, *9*, doi:10.3390/rs9090913.
48. Laliberte, A.S.; Rango, A.; Havstad, K.M.; Paris, J.F.; Beck, R.F.; McNeely, R.; Gonzalez, A.L. Object-oriented image analysis for mapping shrub encroachment from 1937 to 2003 in southern New Mexico. *Remote Sens. Environ.* **2004**, *93*, 198–210, doi:10.1016/j.rse.2004.07.011.
49. Laliberte, A.S.; Goforth, M.A.; Steele, C.M.; Rango, A. Multispectral remote sensing from unmanned aircraft: Image processing workflows and applications for rangeland environments. *Remote Sens.* **2011**, *3*, 2529–2551, doi:10.3390/rs3112529.
50. Yu, Q.; Gong, P.; Clinton, N.; Biging, G.; Kelly, M.; Schirokauer, D. Objectbased detailed vegetation classification with airborne high spatial resolution remote sensing imagery. *Photogramm. Eng. Remote Sensing* **2006**, *72*, 799–811, doi:10.14358/PERS.72.7.799.
51. Baatz, M.; Schäpe, A. Multiresolution Segmentation - an optimization approach for high quality multi-scale image segmentation. *Angew. Geogr. Informationsverarbeitung XII. Beiträge zum Agit.* **2000**, 12–23.
52. Whiteside, T.; Ahmad, W. A Comparison of Object-Oriented and Pixel-Based Classification Methods for Mapping Land Cover in Northern Australia. *Proc. SSC2005 Spat. Intell. Innov. Prax. Natl. Bienn. Conf. Spat. Sci. Inst.* **2005**, 1225–1231.
53. Blaschke, T. Object based image analysis for remote sensing. *ISPRS J. Photogramm. Remote Sens.* **2010**, *65*, 2–16, doi:10.1016/j.isprsjprs.2009.06.004.
54. Niphadkar, M.; Nagendra, H.; Tarantino, C.; Adamo, M.; Blonda, P. Comparing Pixel and Object-Based Approaches to Map an Understorey Invasive Shrub in Tropical Mixed Forests. *Front. Plant Sci.* **2017**, *8*, 1–18, doi:10.3389/fpls.2017.00892.
55. Laliberte, A.S.; Rango, A.; Herrick, J.E.; Fredrickson, E.L.; Burkett, L. An object-based image analysis approach for determining fractional cover of senescent and green vegetation with digital plot photography. *J. Arid Environ.* **2007**, *69*, 1–14, doi:10.1016/j.jaridenv.2006.08.016.
56. Tatjana, Veljanovski; Urša, Kanjir; Krištof, O. Object-based image analysis of remote sensing. *Geod. Vestn.* **2011**, *55*, 665–688.

57. Burnett, C.; Blaschke, T. A multi-scale segmentation / object relationship modelling methodology for landscape analysis. **2003**, *168*, 233–249, doi:10.1016/S0304-3800(03)00139-X.
58. Hall, R.J.; Peddle, D.R.; Klita, D.L. Mapping conifer understory within boreal mixedwoods from Landsat TM satellite imagery and forest inventory information. *For. Chron.* **2000**, *76*, 887–902, doi:10.5558/tfc76887-6.
59. Chastain, R. a; Townsend, P. a Use of Landsat ETM and Topographic Data to Characterize Evergreen Understory Communities in Appalachian Deciduous Forests. *Photogramm. Eng. Remote Sens.* **2007**, *73*, 563–575, doi:10.14358/PERS.73.5.563.
60. Ishii, J.; Washitani, I. Early detection of the invasive alien plant Solidago altissima in moist tall grassland using hyperspectral imagery. *Int. J. Remote Sens.* **2013**, *34*, 5926–5936, doi:10.1080/01431161.2013.799790.
61. Xie, Y.; Sha, Z.; Yu, M. Remote sensing imagery in vegetation mapping: a review. *J. Plant Ecol.* **2008**, *1*, 9–23, doi:10.1093/jpe/rtm005.
62. Liu, Y.; Hill, M.J.; Zhang, X.; Wang, Z.; Richardson, A.D.; Hufkens, K.; Filippa, G.; Baldocchi, D.D.; Ma, S.; Verfaillie, J.; Schaaf, C.B. Using data from Landsat, MODIS, VIIRS and PhenoCams to monitor the phenology of California oak/grass savanna and open grassland across spatial scales. *Agric. For. Meteorol.* **2017**, *237–238*, 311–325, doi:10.1016/j.agrformet.2017.02.026.
63. Salajanu, D.; Jacobs, D.M. Using Forest Inventory Plot Data and Satellite Imagery From Modis and Landsat-Tm To Model Spatial Distribution Patterns of Honeysuckle and Privet. *USDA For. Serv.* **2009**.
64. Caetano, M.; Oliveira, T.; Paúl, J.; Vasconcelos, M.J.; Pereira, J.M.C. Mapping shrublands and forests with multispectral satellite images based on spectral unmixing of scene components. *Proc. SPIE - Int. Soc. Opt. Eng.* **1997**, *3222*, 4–14, doi:10.1117/12.298143.
65. National Capital Commission. Executive Summary: Report on Gatineau Park Ecosystems. Available online: http://s3.amazonaws.com/ncc-ccn/documents/16002_gp_statusreport_summary_e.pdf?mtime=20170504082658 (accessed on 20 January 2018)
66. Del Degan, M. Gatineau Park Ecosystem Conservation Plan; Presented to the National Capital Commission in 2010. Available online: http://s3.amazonaws.com/ncc-ccn/documents/Gatineau-Park-Ecosystem-Conservation-Plan-Summary-Feb-2010.pdf?mtime=20170504083459 (accessed on 14 December 2017)

67. Kandwal, R.; Jeganathan, C. Discriminating the invasive species,'Lantana'using vegetation indices. *J. Indian Soc. Remote Sens.* **2009**, *37*, 275–290, doi:10.1007/s12524-009-0027-5.
68. Knudby, A.J.; Leduc, M.-B. *Tracking the change in wild leek and white trillium distributions in Gatineau Park*; 2017;
69. He, Y.; Nesbitt, N.; Tong, A.; Mui, A. *Delineating the endangered White Trillium (Trillium grandiflorum) and improving Wild leek (Allium tricoccum) mapping using remote sensing and GIS technology in Gatineau Park*; 2012;
70. Li, W.; Guo, Q. A new accuracy assessment method for one-class remote sensing classification. *IEEE Trans. Geosci. Remote Sens.* **2014**, *52*, 4621–4632, doi:10.1109/TGRS.2013.2283082.
71. Li, W.; Guo, Q. How to assess the prediction accuracy of species presence-absence models without absence data? *Ecography (Cop.).* **2013**, *36*, 788–799, doi:10.1111/j.1600-0587.2013.07585.x.
72. POWERS, D.M.W. Evaluation: From Precision, Recall and F-Measure To Roc, Informedness, Markedness & Correlation. *J. Mach. Learn. Technol.* **2011**, *2*, 37–63, doi:10.1.1.214.9232.
73. I.G.O. - Données écoforestières. Ministère des Forêts, de la Faune et des Parcs. Available online: https://geoegl.msp.gouv.qc.ca/igo/mffpecofor/?id=46c36e6514 (accessed on 11 December2018).
74. Markovsky, I.; Van Huffel, S. Overview of total least-squares methods. *Signal Processing* **2007**, *87*, 2283–2302, doi:10.1016/j.sigpro.2007.04.004.
75. Hunt, E.R.; Hively, W.D.; Mccarty, G.W.; Daughtry, C.S.T.; Forrestal, P.J.; Kratochvill, R.J.; Carr, J.L.; Allen, N.F.; Fox-Rabinovitz, J.R.; Miller, C.D. NIR-Green-Blue High-Resolution Digital Images for Assessment of Winter NIR-Green-Blue High-Resolution Digital Images for Assessment of Winter Cover Crop Biomass. *GIScience Remote Sens.* **2011**, *48*, 86–98, doi:10.2747/1548-1603.48.1.86.
76. Li, X.; Shao, G. Object-based urban vegetation mapping with high-resolution aerial photography as a single data source. *Int. J. Remote Sens.* **2013**, *34*, 771–789, doi:10.1080/01431161.2012.714508.
77. Yang, W.; Wang, S.; Zhao, X.; Zhang, J.; Feng, J. Greenness identification based on HSV decision tree. *Inf. Process. Agric.* **2015**, *2*, 149–160, doi:10.1016/j.inpa.2015.07.003.
78. Hassanein, M.; Lari, Z.; El-Sheimy, N. A New Vegetation Segmentation Approach for Cropped Fields Based on Threshold Detection from Hue Histograms. *Sensors* **2018**, *18*, 1–25, doi:10.3390/s18041253.
79. Loidl, M.; Wallentin, G.; Wendel, R.; Zagel, B. Mapping Bicycle Crash Risk Patterns on the Local Scale. *Safety* **2016**, doi:10.3390/safety2030017.

80. Salmivaara, A.; Porkka, M.; Kummu, M.; Keskinen, M.; Guillaume, J.H.A. Exploring the Modifiable Areal Unit Problem in Spatial Water Assessments: A Case of Water Shortage in Monsoon Asia. *Water* **2015**, 898–917, doi:10.3390/w7030898.